ISTANBUL TECHNICAL UNIVERSITY ★ INSTITUTE OF SCIENCE AND TECHNOLOGY

MATHEMATICAL MODELING OF DISLOCATION-FIBER INTERACTIONS IN COMPOSITE MATERIALS

M.Sc. Thesis by
Hayri SEZER

Department : Defense Technologies

Programme : Material, Manufacturing and Design

Thesis Supervisor: Prof. Dr. M. Lütfi ÖVEÇOĞLU

MAY 2009

ISTANBUL TECHNICAL UNIVERSITY ★ INSTITUTE OF SCIENCE AND TECHNOLOGY

MATHEMATICAL MODELING OF DISLOCATION-FIBER INTERACTIONS IN COMPOSITE MATERIALS

M.Sc. Thesis by
Hayri SEZER
(514051004)

Date of submission : 19 April 2009
Date of defence examination: 07 May 2009

Supervisor (Chairman) : Prof. Dr. M. Lütfi ÖVEÇOĞLU (ITU)
Members of the Examining Committee : Asc. Prof. Dr. Gültekin GÖLLER (ITU)
Asc. Prof. Dr. H. Süleyman TÜRKMEN (ITU)

MAY 2009

İSTANBUL TEKNİK ÜNİVERSİTESİ ★ FEN BİLİMLERİ ENSTİTÜSÜ

KOMPOZİT MALZEMELERDE DİSLOKASYON-FİBER ETKİLEŞMESİNİN MATEMATİKSEL OLARAK MODELLENMESİ

YÜKSEK LİSANS TEZİ
Hayri SEZER
(514051004)

Tezin Enstitüye Verildiği Tarih : 19 Nisan 2009
Tezin Savunulduğu Tarih : 7 Mayıs 2009

Tez Danışmanı : Prof. Dr. M. Lütfi ÖVEÇOĞLU (İTÜ)
Diğer Jüri Üyeleri : Doç. Dr. Gültekin GÖLLER (İTÜ)
Doç. Dr. H. Süleyman TÜRKMEN (İTÜ)

MAYIS 2009

FOREWORD

It is quite good to work and study and to be guided by people who can understand you and who can support you according to your abilities, so for me it was a great chance and great honour to study with Prof. M. Lütfi ÖVEÇOĞLU. I would like to thank him sincerely for his support, guidance and encouragement.

Family is always very important for us to be succesful in any subject. For this case, I would like to thank my Family for their endless supports.

May 2009

Hayri SEZER

Physics Engineer

TABLE OF CONTENTS

Page

ABBREVIATIONS

$\boldsymbol{b}$	**:** Burgers vector of edge dislocations on the slip plane of the matrix phase
$\boldsymbol{\mu_1, \mu_2}$	**:** Shear modul of the matrix and the in fiber phases
$\boldsymbol{v_1, v_2}$	**:** Poisson's ratios of the matrix and the fiber phases
$\boldsymbol{\tau_{app}}$	**:** Applied or resolved shear stress on the glide palne of the matrix phase
$\boldsymbol{K}$	: $3 - v$
$\boldsymbol{\Gamma}$	: μ_2/μ_1
$\boldsymbol{\alpha}$	: $[\Gamma(K_1 + 1) - (K_2 + 1)]/[\Gamma(K_1 + 1) + (K_2 + 1)]$
$\boldsymbol{\beta}$	: $[\Gamma(K_1 - 1) - (K_2 - 1)]/[\Gamma(K_1 + 1) + (K_2 + 1)]$
$\boldsymbol{C_1}$	: $(\alpha + \beta^2)/(1 - \beta^2)$
$\boldsymbol{C_2}$	: $2(\alpha - \beta)/(1 + \beta)$
$\boldsymbol{C_3}$	: $2(1 + \alpha)\beta/(1 - \beta^2)$
$\boldsymbol{D}$	: $2\mu_1 b/\big(\pi(K_1 + 1)\tau_{app}\big)$; scaling factor
$\boldsymbol{n, N}$	**:** Number of dislocation in pile up

LIST OF TABLES

Page

LIST OF FIGURES

Page

MATHEMATICAL MODELING OF DISLOCATION-FIBER INTERACTIONS IN COMPOSITE MATERIALS

SUMMARY

The aim of this study is to find positions of multiple edge dislocations in a pile-up against a circular/cylindrical interface. During computational procedure, the elasticity solution of Dundurs equation, which is a non linear equation, was utilized. Firstly, Airy function was obtained in cartesian coordinates, then it was calculated in polar coordinates to obtain stress function on cylindrical fiber surface for one edge dislocation against cylindrical fiber surface. For multiple edge dislocations, a general dimensionless mathematical function was obtained. An optimization procedure was applied for the solution of nonlinear equations. For multiple edge dislocations, there are multiple nonlinear equations. In this study, a general code was written for the solution of Dundurs equation and a specific case was investigated (in which number of dislocation was taken as 30). For 30 dislocations, 30 nonlinear equations had been optimized.

The position of discrete dislocations in a fiber composite depends on some different parameters, such as applied stress, fiber radius, shear modulus of matrix and fiber phases…etc. Applied stress can be very important for dislocations positions. In this study, two very important cases will be investigated. Firstly, the effect of varying η_{app}/μ_1 (dimensionless applied stress) for tip shear stress and secondly the effect of changing microstructure, varying Λ (dimensionless pile-up length) for tip shear stress will be investigated. In addition, the optimization will be applied for three different composites, Al/Al_2O_3, Cu/WC and Al/SiC.

KOMPOZİT MALZEMELERDE DİSLOKASYON-FİBER ETKİLEŞMESİNİN MATEMATİKSEL OLARAK MODELLENMESİ

ÖZET

Bu çalışmanın amacı, kompozit malzemelerde N adet ayrık kenar dislokasyonuna uygulanan kayma gerilmesi sonucu dislokasyonların fiber yüzeyine olan uzaklığını bulmaktır. Dislokasyonların fiber çapına olan uzaklıkları için Dundurs"ın bulmuş olduğu, dislokasyon-fiber geometrisinden yararlanılarak oluşturulmuş Airy fonksiyonunun elastic çözümü kullanıldı. Airy fonksiyonu öncelikle kartezyen koordinat sisteminde oluşturuldu. Daha sonra Airy fonksiyonu polar koordinat sisteminde yazıldı. Polar koordinat sisteminde yazılmış olan Airy fonksiyonu kullanılarak silindirik fiber yüzeyinde meydana gelen gerilme polar koordinatlarda hesaplandı. Elde edilen denklem boyutsuzlaştırılarak matematiksel bir denklem elde edildi. Elde edilen denklem çoklu dislokasyon sistemi için yeniden yazılarak genel bir denklem elde edildi. Bu denklem lineer olmayan karmaşık bir denklem olduğundan optimizasyon yöntemi uygulandı. N tane ayrık kenar dislokasyonu için N tane linear olmayan denklem vardır. Bu çalışma için genel bir kod yazıldı. Fakat 30 tane dislokasyon için optimizasyon işlemi yapıldı.

Fiber kompozitlerde ayrık dislokasyonların yerleri (uygulanan bir gerilim altında fiber yüzeyine olan mesafeleri); uygulanan gerilme, fiber çapı, anafazın kayma gerilmesi ve fiber fazların kayma modülleri gibi parametrelere bağlıdır. Bu çalışmada iki önemli durum incelenecektir. Bunlardan birincisi kayma düzlemindeki kayma gerilmesi, uygulanan boyutsuz gerilmeye bağlı olarak incelenecektir. İkinci durumda ise kayma düzlemindeki kayma gerilmesi, elde edilen boyutsuz dislokasyon yığılma konumlarına bağlı olarak incelenecektir. Aynı zamanda, optimizasyon üç farklı kompozit, Al/Al_2O_3, Cu/WC ve Al/SiC, için uygulanacaktır.

1. INTRODUCTION

Computational methods in material science and engineering is one of the most essential point to understand micro structure of materials, because of fact that material modeling is one of the fastest growing areas in the science and engineering of materials [1]. The need for efficient computational performance is crucial not only in basic science but also in almost all areas of technological applications [2]. Microstructures of materials are very essential to understand mechanical behaviors of materials and especially dislocations play a vital role for mechanical behaviors of materials. Because, the motion of dislocations leads to plastic deformation in crystals. When single crystals are stressed, they undergo plastic deformation when the stress is high enough. However, the critical stress in a real material is several orders of magnitude lower than the theoretical stress to shear a perfect crystal [3]. Dislocations are the elementary carriers of plastic flow. The ultimate aim of dislocation theory is the prediction of the mechanical properties of crystalline materials [4]. In this study, a discrete dislocation modeling was used to understand the effect of varying τ_{app}/μ_1 (dimensionless applied stress) for tip shear stress and the effect of changing microstructure, varying Λ (dimensionless pile-up length) for tip shear stress.

The problem of a dislocation pile-up near the boundary of a second phase is a classical one studied and interpreted as a basic model for analyzing certain phenomena such as work hardening, yielding, and crack nucleation [5] and fiber failure. Eshelby, Frank and Nabarro [6] who calculated the equilibrium positions of N discrete dislocations piled-up behind a locked dislocation in an infinite, single-phase isotropic linear elastic solid subjected to uniform remote shear loading studied the first theoretical analysis of a simple pile-up configuration. After the solution of Eshelby, Frank and Nabarro, Stroh [7] find out the local stresses about the leading edge of the pile-up and studied the feasibility of micro crack nucleation ahead of a blocked slip band, which was defined like Eshelby, Frank and Nabarro (EFN) solution. Leibfried [8], Haasen and Leibfried, Head and Louat and Head [5] found

that, when N is large calculations involving linear pile-ups are most easily treated by replacing the discrete dislocations in the array by a continuous distribution of dislocations of infinitesimal Burgers vectors; in infinite single phase problems, the sought distribution is obtained by solving a singular integral equation of the Cauchy type, which is usually straightforward to analytically perform. Numerical solution of this equation is a standard problem that there are many numerical solution examples in literature [9]. When dislocation pile-ups in different two phases solids are considered, the continuous distribution approach leads to singular integral equations whose kernels are no longer of the pure Cauchy type. For a single screw dislocation pile-up perpendicular to the interface between two dissimilar isotropic half-spaces, Barnett [5] has obtained a closed-form analytical solution for the associated dislocation distribution and pile-up stresses. Kuang and Mura [10] treated the corresponding problem for an edge dislocation array using a Wiener-Hopf technique; this method yields a closed-form solution of such complexity that one is persuaded that a direct numerical method might have been a more prudent approach for generating the solution. Tucker [5] studied in this subjects and he showed that the Wiener-Hopf method may also be used to treat a screw pile-up inclined to an interface (including possible elastic anisotropy); except for asymptotic stresses near the pile-up tip, substantial effort is required to numerically evaluate the closed-form results. That it can be stated for the solution of dislocation, pile-up in two-phase media the continuous dislocation distribution approximation does not have any essential advantages, because the numerical solution of continuous distribution approximation is very difficult and unuseful for dislocation pile-ups. Discrete dislocation approximation is an easier and more straightforward approach for dislocation pile-ups problems that is like in crystalline media. The N dislocations positions must be found by solving N nonlinear algebraic equations. This method is relatively easy duty for present computational techniques. N nonlinear algebraic equation is not a system of nonlinear equations. For N dislocations, there are N different nonlinear equations with 1, 2… N unknowns. For example, for the 1th nonlinear equation there is only one unknown, for 2nd nonlinear equation there are 2 unknowns and for Nth nonlinear equation there are N unknowns.

These kinds of system of equations generally are smiliar with engineering optimization problems. Furthermore, this method allows the problem to be easily formulated, is reasonably transparent, and is valid when N is small and the continuous distribution approximation is uncertain.

This study treats the equilibrium conditions for a pile-up of discrete edge dislocations in a fiber composite. The formulation of the problem and the solutions for the equilibrium standoff distances and the shear stress acting on the slip plane are all based on the elasticity solution described by the Airy stress function formulated by Dundurs [5] for the same solid with only one edge dislocation example. Airy stress function was used to reformulate the equilibrium equations for multiple edge dislocations under an applied shear stress and a given set of elastic parameters and equilibrium equations were solved. The equilibrium positions of multiple edge dislocations pile up against a fiber in a composite determined numerically in Matlab Optimization toolbox with fminunc algorithm. The problem was taken as an unconstrained optimization problem. In this study, large-scale fminunc algorithm was utilized since the nonlinear equation is very long and the convergence of each root was very difficult. During the optimization process, some roots converged to infinity. In order to ignore this case, hessian and gradient of Airy function had to be defined. Understanding composite materials failure is beneficial for aerospace, military, commercial, materials, energy, transportation and other industrial, so the aim of this study has been to develop a better understanding of mathematical modeling for dislocations effects in a fiber failure in composite materials.

2. COMPOSITE MATERIALS

2.1 Composites

The word composite in the term composite material signifies that two or more materials are combined on a macroscopic scale to form a useful third material [11]. Composites exist in nature. A piece of wood is a composite, with long fibers of cellulose (a very complex form of starch) held together by a much weaker substance called lignin [12]. Cellulose is also found in cotton and linen, but it is the binding power of the lignin that makes a piece of timber much stronger than a bundle of cotton fibers. Humans have been using composite materials for thousands of years. Take mud bricks for example. A cake of dried mud is easy to break by bending, which puts a tension force on one edge, but makes a good strong wall, where all the forces are compressive. A piece of straw, on the other hand, has a lot of strength when one tries to stretch it but almost none when one crumbles it up. If pieces of straw were embedded in a block of mud and was let dry hard, the resulting mud brick resists both squeezing and tearing and makes an excellent building material. Put more technically, it has both good compressive strength and good tensile strength [12]. The necessity of inventing composite materials is to get both high specific strength and high specific modulus properties joined in one material. Composite materials generally have many superior mechanical properties such as high strength, high fatigue strength, excellent wear resistance, high thermal capacity, high corrosion resistance, suitable thermal and electrical conductivity and low weight [13].

Materials properties in composite materials affect the properties of composites. Such as, physical and mechanical properties. Production of composite and production cost is very expensive and composite materials are not recyclable. Because of this all facts, selection of materials is essential to obtain expected properties of composites.

Composite materials are composed of two or more distinct phases (matrix phase and dispersed phase) and having bulk properties significantly different form those of any of the constituents [14]. Matrix phase is the primary phase, having a continuous

character, is called matrix. Matrix is usually more ductile and less hard phase. It holds the dispersed phase and shares a load with it. Dispersed (reinforcing) phase is the second phase (or phases) and imbedded in the matrix in a discontinuous form. This secondary phase is known as dispersed phase. Dispersed phase is usually stronger than the matrix, therefore it is sometimes called the reinforcing phase.

Many of common materials (metal alloys, doped Ceramics and Polymers mixed with additives) also have a small amount of dispersed phases in their structures, however they are not considered as composite materials since their properties are similar to those of their base constituents (physical properties of steel are similar to those of pure iron). There are two classification systems of composite materials. One of them is based on the matrix material (metal, ceramic and polymer) and the second is based on the material structure [14].

2.2 Classification of Composites

2.2.1 Matrix Material Base

2.2.1.1 Metal Matrix Composites (MMC)

Examples of metal matrix composites stretch back to the ancient civilizations. Copper awls from Cayonu (Turkey) date back to about 7000 BC [15]. Metal-matrix composites are either in use or in prototyping for the Space Shuttle, commercial airliners, electronic substrates, bicycles, automobiles, golf clubs, and a variety of other applications. While the vast majority is aluminum matrix composites, a growing number of applications require the matrix properties of super alloys, titanium, copper, magnesium, or iron [16]. MMCs are made by dispersing a reinforcing material into a metal matrix. The reinforcement surface can be coated to prevent a chemical reaction with the matrix. The principal matrix materials for MMCs are aluminum and its alloys. To a lesser extent, magnesium and titanium are also used, and for several specialized applications a copper, zinc or lead matrix may be employed [17]. For example, carbon fibers are commonly used in aluminum matrix to synthesize composites showing low density and high strength [10]. However, carbon reacts with aluminum to generate a brittle and water-soluble compound Al_4C_3 on the surface of the fiber. To prevent this reaction, the carbon fibers are coated with nickel or titanium boride [10].

2.2.1.2 Ceramic Matrix Composites (CMC)

Ceramic matrix composites (CMCs) combine reinforcing ceramic phases with a ceramic matrix to create materials with new and superior properties [18]. A given ceramic matrix can be reinforced with either discontinuous reinforcement, such as particles, whiskers or chopped fibers, or with continuous fibers [19]. In the first case, the enhancement of the mechanical properties, in terms of failure strength and toughness, is relatively limited but it can be significant enough for specific applications, a well-known example being the use of ceramics reinforced with short fibers in the field of the cutting tools (SiCw/Si3N4 composites). Among the discontinuous reinforcements, whiskers are by far the most attractive in terms of mechanical properties. Unfortunately, their use raises important health problems both during processing and in service.

Conversely, continuous reinforcements, such as fiber yarns, are much more efficient, from a mechanical standpoint, but they are more expensive and more difficult to use in a ceramic matrix in terms of material design and processing [20].

2.2.1.3 Polymer Matrix Composites (PMC)

Polymer-matrix composites consist of glass, carbon, or other high-strength fibers in a thermoset or thermoplastic resin. The resulting materials are strong, stiff, and corrosion resistant. PMCs adopt flat, gently curved, or sharply sculpted contours with ease, providing manufacturers with design flexibility [21]. Use of non-reinforced polymers as structure materials is limited by low level of their mechanical properties: tensile strength of one of the strongest polymers-epoxy resin is 20000 psi (140 MPa). In addition to relatively low strength, polymer materials possess low impact resistance [14].

2.2.2 Reinforcing Material Structure Base

2.2.2.1 Particulate Composites

A particle has no long dimension. Particle composites consist of particles of one material dispersed in a matrix of a second material. Particles may have any shape or size, but are generally spherical, ellipsoidal, polyhedral, or irregular in shape [22].

Particle-reinforced composites are candidate materials for a wide variety of aerospace and nonaerospace applications. High costs and technical difficulties involved with the use of many fiber-reinforced composites often limit their use in many applications [23]. Consequently, particulate composites have emerged as viable alternatives to conventional fiber-reinforced composites. Particulate composites can be processed to near net shape potentially reducing the manufacturing costs. They are candidate materials where shock or impact properties are important. For example, particle-reinforced metal matrix composites have shown great potential for many automotive applications [24]. Typically, these materials are aluminum matrix reinforced with SiC or TiC particles. Reinforced concrete can also be thought of as a particle-reinforced composite. In situ ceramics can be modeled as particulate composites and are candidate materials for many high-temperature applications. The characterization of these materials is fundamental to their reliable use [25].

2.2.2.2 Fibrous Composites

Fibers (or wires) of various types are stronger a long their lengths than the same material in bulk form. This is due to the small cross-sectional dimensions of fibers, thus minimizing the inherent presence of molecular imperfections, flaws and dislocations. The common fiber used for engineering applications are glass, carbon (graphite) and kevlar (aramid). The reinforcing fibers (the discontinuous medium) in the fiber composites should be desirably have the following properties [26].

- A high modulus of elasticity in the direction of the fiber.
- A high ultimate strength in the direction of the fiber.
- A low variation of mechanical properties between individual fibers.
- Stability and retention of mechanical properties during handling and fabrication.
- Uniform fiber cross-section

Fibers by themselves are useless for structural engineering applications unless they are bound together to form a structural element capable of withstanding loads. The binding material is called the matrix. The matrix should have the following properties [26].

- Bind the fibers together.
- Transfer the applied loads to fibers
- Stop, to some extent, a crack from propagating straight through a mass of fibers.
- Protect the fibers surfaces from damage during handling and in service, including the environment
- Be chemically and thermally compatible with fibers.

The most widely used matrix for fibrous composites are the organic 'super polymer' materials, commonly called plastics. Fibrous composites are usually laminated, that is the individual layers of the material are bonded together for form an element or plate. Layers of fiber-reinforced material are built-up with the fibers.
When the constituent materials in each layer are the same, the laminated layers are called a 'laminate'. If the layer is of different constituent materials, or of the same materials, but different fiber reinforcing pattern, the laminate is then said to be a 'hybrid laminate'. The study of mechanic of fibrous composites is divided into two broad areas, continuous fibers and short fibers. The length of the reinforcing fiber affects the structural behaviors of the composite. In this study, a mathematical modeling of dislocation effect in fiber composites materials was investigated with numerical solutions [26].

2.3 Application of Composite Materials

Composite materials have seen an increasing number of applications, not only in military applications but also in commercial ones. Composites are mostly used in defecence industry. Composite materials have been used extensively in military aircraft since the mid 1970s. Application of composites, mostly in defence industry is shown in Figure 2.1. Commercial aircraft are currently under design and manufacture (e.g., Airbus 380 and Boeing 7E7) that will make extensive use of composite materials. Up to 60% of the structure of the 7E7 will be composite materials.

Figure 2.2 shows application of materials for different industrial and defence fields [27]. The importance of the composites forced me to study in this field. It is an inter discipline fields that can be applied in wide areas.

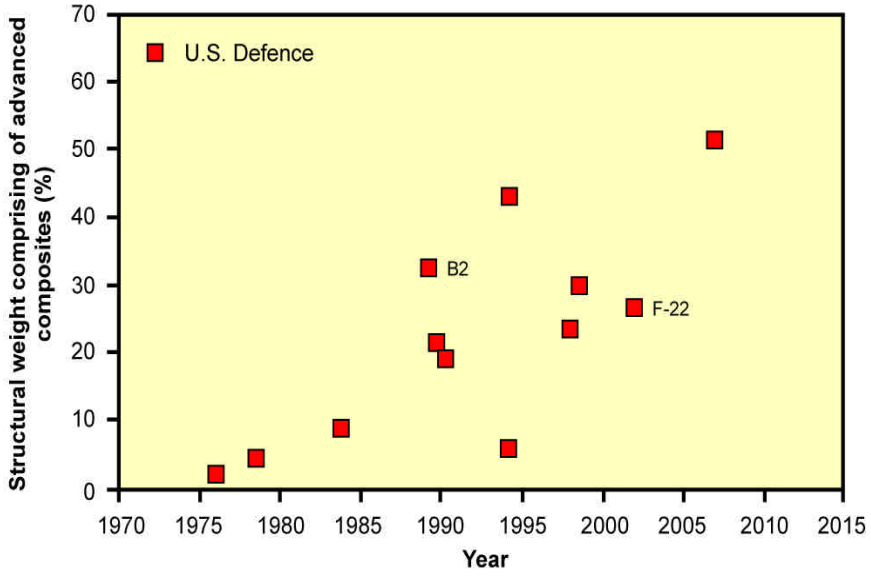

Figure 2.1: Application of composites in defence industry

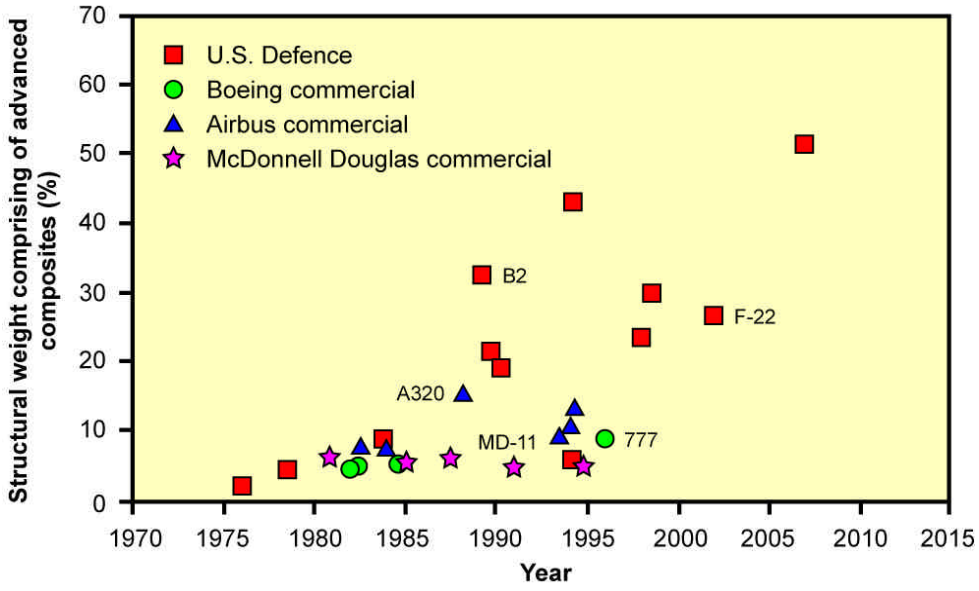

Figure 2.2: Application of composite materials

3. DISLOCATIONS

3.1 Crystalline Materials

Dislocations are linear defects in crystalline solids [28], and elementary understanding of crystalline is required before dislocations can be introduced. Metals and many important classes of nonmetallic solids are crystalline, i.e. the constituent atoms are arranged in a pattern that repeats itself periodically in three dimensions [29]. The actual arrangement of the atoms is described by the crystal structure. The crystal structures of most pure metals are simple, the three most common being the body-centered cubic, face-centered cubic and close-packed hexagonal structures [30]. However, the structures of alloys and non-metallic compounds are often complex. The arrangement of atoms in a crystal can be described with respect to a three-dimensional net formed by three sets of straight, parallel lines as in Fig. 3.1(a). The lines divide space into equal sized parallelepipeds and the points at the intersection of the lines define a space lattice [31]. Every point of a space lattice has identical surroundings. Each parallelepiped is called a unit cell and the crystal is constructed by stacking identical unit cells face to face in perfect alignment in three dimensions. By placing a motif unit of one or more atoms at every lattice site the regular structure of a perfect crystal is obtained [32]. The positions of the planes, directions and point sites in a lattice are described by reference to the unit cell and the three principal axes, x, y and z Fig. 3.1(b)

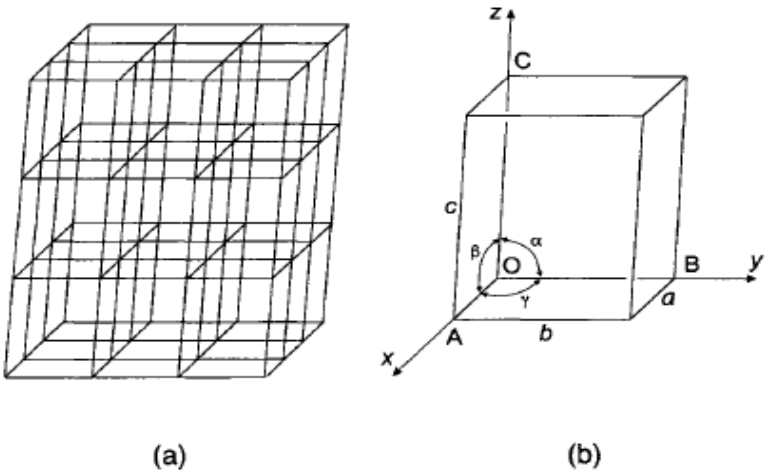

Figure 3.1: (a) A space lattice, (b) unit cell showing positions of principal axes.

3.2 Defects in Crystalline Materials

All real crystals contain imperfections which may be point, line, surface or volume defects as and which disturb locally the regular arrangement of the atoms figure 3.2. Their presence can significantly modify the properties of crystalline solids, and although this study is primarily concerned with the line defects, namely dislocations, it will be seen that the behavior and effects of all these imperfections are intimately related [33].

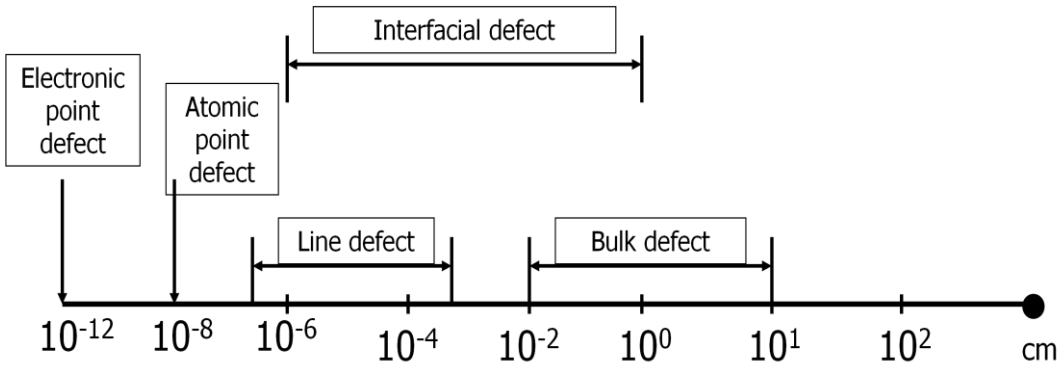

Figure 3.2: Relative size ranges of defects [12].

3.3 Line Defects: Dislocations

The subject of dislocations is essential for an understanding of many of the physical and mechanical properties of crystalline solids. In materials science, a dislocation is a crystallographic defect, or irregularity, within a crystal structure [34]. The presence of dislocations strongly influences many of the properties of materials. Vito Volterra originally developed the theory in 1905. Some types of dislocations can be visualized as being caused by the termination of a plane of atoms in the middle of a crystal. In such a case, the surrounding planes are not straight, but instead bend around the edge of the terminating plane so that the crystal structure is perfectly ordered on either side. The analogy with a stack of paper is apt: if a half a piece of paper is inserted in a stack of paper, the defect in the stack is only noticeable at the edge of the half sheet. There are two primary types: edge dislocations and screw dislocations. Mixed dislocations are intermediate between edge and screw dislocations [31].

3.3.1 Edge Dislocations

The simplest type of dislocation, which was originally suggested by Orawan, Polanyi and Taylor is called edge dislocation or Taylor-Orawan dislocation [31]. The dislocation shown Fig. 3.6(a) is an edge dislocation, which is located at the edge of an extra half plane of atoms. Figure 3.3 shows the slip that produces an edge dislocation for an element of crystal having a simple cubic lattice. Slip has occurred in direction of the slip vector over the area ABCD. The boundary between the right-hand slipped part of the crystal and left-hand part, which has not yet slipped, is the line AD of the edge dislocation. In the direction of the slip with respect to the part of the crystal below the slip plane by an amount indicated by shaded area in figure 3.3. the amount of displacement is equal to the Burger vector **b** of the dislocation. The characteristic definition of an edge dislocation is that its burgers vector is always perpendicular to dislocation line.

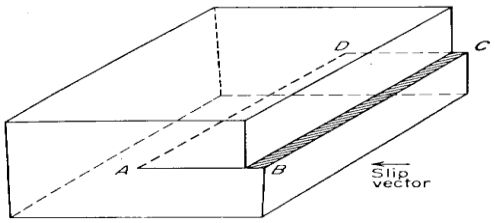

Figure 3.3: Edge dislocation produced by slip in a simple cubic lattice. Dislocation lies along AD, perpendicular to slip direction. Slip has occured over area ABCD[35].

Despite the exact arrangement of atoms along AD is not known, it can be generally like in Figure 3.4 closely represent the atomic arrangement in a plane normal to edge dislocation AD. The place of the paper in this figure corresponds to a (100) plane in a simple cubic lattice and is equivalent to any plane parallel to the front face of figure 3.3. There is one more vertical row of atoms above the slip planet han below it. The atomic arrangement results in a compressive stress above the slip plane and a tensile stress below the slip plane. And edge dislocation with extra plane of atoms above the slip plane, as in figure 3.4, by convention is called a positive edge dislocation and is generally indicated by the symbol (⊥) If the extra plane of atoms lies below the slip plane, the dislocation is a negative edge dislocation and it is generally indicated by the symbol(⊤)

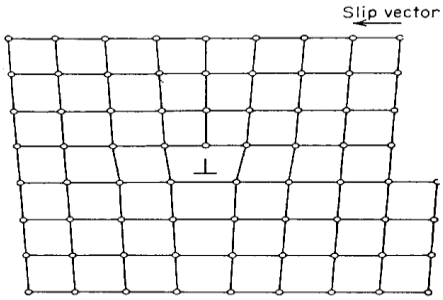

Figure 3.4: Atomic arrangement in a plane normal to an edge dislocation [35].

A pure edge dislocation can glide or slip in a direction perpendicular to its length. However, it may move vertically by a process known as climb, if diffusion of atom or vacancies can take place at an appreciable rate. Think about figure 3.4. For the edge dislocation to move upward, it is necessary to remove the extra atom directly over the symbol (⊥) figure 3.5 or to add a vacancy to this spot. One such atom would have to be removed for every atomic spacing that the dislocation climbs. Conversely, if the dislocation moved in down direction atoms would have to be added. Atoms could be removed from extra plane of atoms by the extra atom interacting with a

lattice vacancy. Atoms are added to the extra plan effort negative climb by the diffusion of an atom from the surrounding crystal, creating a vacancy. Since movement by climb is a diffusion controlled, motion is much slower than in glide and less likely except at high temperatures.

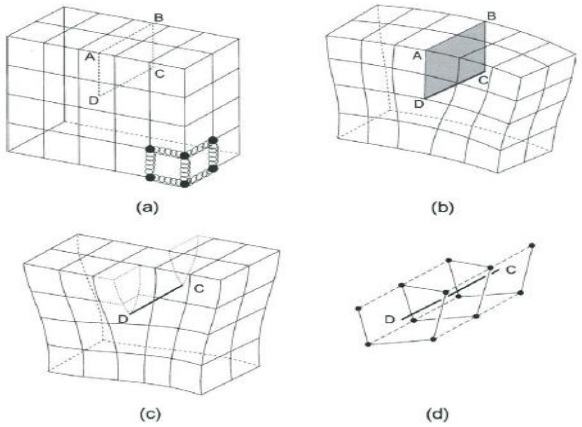

Figure 3.5: (a) Model of a simple cubic lattice; the atoms are represented by filled circles, and the bonds between atoms by springs, only a few of which are shown; (b) positive edge dislocation DC formed by inserting an extra half-plane of atoms in ABCD; (c) left-handed screw dislocation DC formed by displacing the faces ABCD relative to each other in direction AB; (d) spiral of atoms adjacent to the line DC in (c) [33].

3.3.2 Screw Dislocations

An example is shown in Fig. 3.6(b), which is created by a similar "cut-and-slip" operation except that the slip direction is now parallel to the dislocation line. This dislocation is called screw because the atoms around the line are arranged in a spiral, as shown by the white arrows in Fig. 3.6(b). The most important characteristic properties of screw dislocations can be defined as, a screw dislocation lies parallel to the burgers vector and a screw dislocation moves (in the slip plane) in a direction perpendicular to the burgers vector (slip direction) [36].

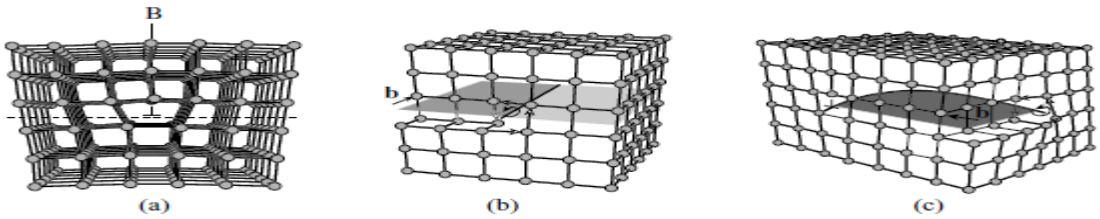

Figure 3.6: (a) An edge dislocation created by inserting a half-plane of atoms. (b)A screw dislocation created by a "cut-and-slip" procedure in which the slip vector is parallel to the dislocation line. The slipped area of the cut plane is shown in dark gray and the un-slipped area is shown in light gray. The dislocation line is marked by the solid line. (c) A curved dislocation line with an edge orientation at one end (on the left) and a screw orientation at the other end (on the right) [37].

3.3.3 Mixed Dislocations

Dislocations with orientations between screw and edge, such as the curved line in Fig. 1.5(c), are called mixed dislocations. The angle between the dislocation line and the slip vector is called the character angle. The character angle is 0◦ for a screw dislocation, 90◦ for an edge dislocation, and between 0◦ and 90◦ for a mixed dislocation.

3.3.4 Burger Vector

A burgers circuit consists of a sequence of jumps from atoms to their neighbors. The burgers circuit should form a complete loop when it is drawn in a perfect crystal. When the same Burgers circuit is drawn in a defective crystal, it may not end at the starting atom. When this happens, the vector pointing from the starting atom to the ending atom gives a measure of topological mis-connection of the defective crystal structure. At a first glance, such a test may appear to be rather arbitrary since there is so much freedom in choosing the Burgers circuit. Remarkably, the resulting mis connection vector turns out to be the same (modulo sign) for any circuit that encloses the same dislocation. Let us try the Burgers circuit test on a two-dimensional plane of atoms perpendicular to an edge dislocation, as shown in Figure 3.7. The analysis that follows is easy to extend to more complex three-dimensional atomic structures. To set a sign convention, let us agree on the flow direction for the test circuit. The common convention is to first select a direction or sense, ξ , for the dislocation line.

Then, the flow direction for the test circuit is defined with respect to the chosen line sense following the right-hand-rule. The sense direction ξ is arbitrary and here we choose it to point out of the paper. According to our convention, the Burgers circuit flows counterclockwise.

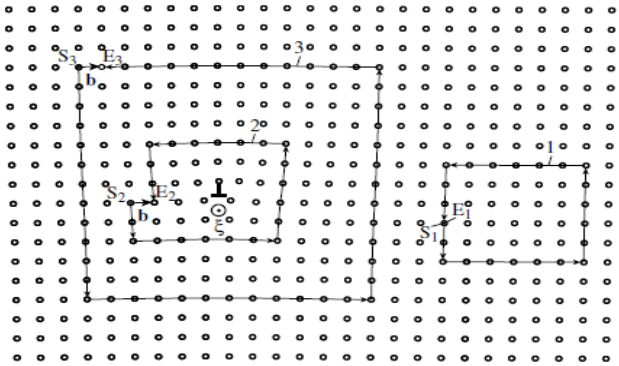

Figure 3.7: Three Burgers circuits drawn on an atomic plane perpendicular to an edge dislocation in a SC crystal. The start and ends of the circuits are Si and Ei, respectively. Circuit 1 does not enclose dislocation ⊥ whereas circuits 2 and 3 do. The sense vector $\boldsymbol{\xi}$ is defined to point out of the paper so that all three circuits flow in the counterclockwise direction [37].

4. DISLOCATION MODELLING

4.1 Introduction

Micromechanical modeling of solids is essential to understand macro behaviors of materials. This importance has been fueled by the realization that many materials have heterogeneous microstructures that play a dominant role in determining macro deformational behavior. Materials where this occurs include multiphase fiber and particulate composites, soil, rock, concrete, and various granular materials. These materials have microstructures that occur at a variety of length scales from meters to nanometers, and general interest lies with the case where the length scale is smaller than other characteristic lengths in the problem. The response of such heterogeneous solids shows strong dependence on the micromechanical behaviors between different material phases. Classical theories of continuum mechanics have limited ability to predict such behaviors, and this has lead to the development of many new micromechanical theories of solids. Therefore, the discrete dislocation modeling is very important to understand complexity of micromechanics of materials [38].

4.2 Elasticity

4.2.1 Linear Elasticity Theory for Plasticity

The mechanical interaction between different dislocations (2D case) or different dislocation segments (3D case) is transmitted by the constituent elements (atoms) of the material. In this approach, the material is described as an isotropic or anisotropic linear elastic unbounded homogeneous continuum in which the dislocations are embedded as elementary carriers of displacement and stress. This statement already implies some essentials associated with the mathematical treatment of dislocations, namely, that they are outside their cores simulated as line defects in the framework of linear elasticity. Large strains occurring close to the dislocation cores are naturally excluded from the elastic treatment.

For this purpose, an inner cutoff radius in the order of the magnitude of the Burgers vector is used. The dislocations are generally treated as stationary defects, that is, their displacement field does not depend on time [39].

4.2.2 Hooke's law

Objects that quickly regain their original shape after being deformed by a force, with the molecules or atoms of their material returning to the initial state of stable equilibrium, often obey Hooke's law. We may view a rod of any elastic material as a linear spring. The rod has length L and cross-sectional area A. Its extension (strain) is linearly proportional to its tensile stress, σ by a constant factor, the inverse of its modulus of elasticity, E, hence

$\sigma = E\varepsilon$ or **(4.1)**

$\Delta L = \frac{F}{EA}L = \frac{\sigma}{E}L$ **(4.2)**

Hooke's law only holds for some materials under certain loading conditions. Steel exhibits linear-elastic behavior in most engineering applications; Hooke's law is valid for it throughout its elastic range (i.e., for stresses below the yield strength). For some other materials, such as aluminum, Hooke's law is only valid for a portion of the elastic range.

For some materials a proportional limit stress is defined, below which the errors associated with the linear approximation are negligible. Applications of the law include spring operated weighing machines, stress analysis and modeling of materials [40].

4.2.2.1 Tensor expression of Hooke's Law

When working with a three-dimensional stress state, a 4th order tensor (C_{ijkl}) containing 81 elastic coefficients must be defined to link the stress tensor (σ_{ij}) and the strain tensor (or Green tensor) (ε_{kl}).

$\sigma_{ij} = \sum_{kl} C_{ijkl}.\varepsilon_{kl}$ **(4.3)**

Due to the symmetry of the stress tensor, strain tensor, and stiffness tensor, only 21 elastic coefficients are independent. As stress is measured in units of pressure and strain is dimensionless, the entries of cijkl are also in units of pressure. Models of

neo-Hookean solids and Mooney-Rivlin solids provide generalization for the case of large deformations.

Physical equations involving isotropic materials must therefore be independent of the coordinate system chosen to represent them. The strain tensor is a symmetric tensor. Since the trace of any tensor is independent of coordinate system, the most complete coordinate-free decomposition of a symmetric tensor is to represent it as the sum of a constant tensor and a traceless symmetric tensor.

$$\varepsilon_{ij} = \left(\frac{1}{3}\varepsilon_{kk}\delta_{ij}\right) + \left(\varepsilon_{ij} - \frac{1}{3}\varepsilon_{kk}\delta_{ij}\right) \quad \textbf{(4.4)}$$

where δ_{ij} is the Kronecker delta. The first term on the right is the constant tensor, also known as the pressure, and the second term is the traceless symmetric tensor, also known as the shear tensor. The most general form of Hooke's law for isotropic materials may now be written as a linear combination of these two tensors:

$$\sigma_{ij} = 3K\left(\frac{1}{3}\varepsilon_{kk}\delta_{ij}\right) + 2G\left(\varepsilon_{ij} - \frac{1}{3}\varepsilon_{kk}\delta_{ij}\right) \quad \textbf{(4.5)}$$

where K is the bulk modulus and G is the shear modulus. Using the relationships between the elastic module, these equations may also be expressed in various other ways. For example, the strain may be expressed in terms of the stress tensor as:

$$\left.\begin{aligned}
\varepsilon_{11} &= \frac{1}{E}\left(\sigma_{11} - v(\sigma_{22} + \sigma_{33})\right)\\
\varepsilon_{22} &= \frac{1}{E}\left(\sigma_{22} - v(\sigma_{11} + \sigma_{33})\right)\\
\varepsilon_{33} &= \frac{1}{E}\left(\sigma_{33} - v(\sigma_{11} + \sigma_{22})\right)\\
\varepsilon_{12} &= \frac{\sigma_{12}}{2G}\\
\varepsilon_{13} &= \frac{\sigma_{13}}{2G}\\
\varepsilon_{23} &= \frac{\sigma_{23}}{2G}
\end{aligned}\right\} \quad \textbf{(4.6)}$$

Where, E is the modulus of elasticity and ν is Poisson's ratio [41].

4.3 Plane Strain

In isotropic elasticity theory, and in particular for finite bodies where image effects must be considered, the mathematical complexity is considerable. For plane stress or strain the treatment simplifies a great deal. Of these simple cases, plane strain is discussed as an example because of its importance in the theory of straight dislocations. Plane strain is produced in a body under a state of stress such that there is no dependence of the displacements on one coordinate, say x_3, and such that the displacement u_3 is zero [42]. Thus

$$u_1 = u_1(x_1, x_2) \quad u_2 = u_2(x_1, x_2) \quad u_3 = 0 \text{ and } \frac{\partial}{\partial x_3} \tag{4.7}$$

$$\frac{\partial \sigma_{1i}}{\partial x_1} + \frac{\partial \sigma_{2i}}{\partial x_2} + \frac{\partial \sigma_{3i}}{\partial x_3} + f_i = 0 \;\; i = 1,2,3 \tag{4.8}$$

With the conditions of Equations (4.7), the essential description of plane strain derives from the equilibrium equations (4.8). In applications we are interested primarily in the state of internal strain in an infinitesimal volume element lying within the isotropic continuum and not acted on by body forces. Equations (4.8) and (4.7) then combine to the form (in cartesian or polar coordinates)

$$\frac{\partial \sigma_{11}}{\partial x_1} + \frac{\partial \sigma_{12}}{\partial x_2} = 0 \;\; or \;\; \frac{\partial \sigma_{rr}}{\partial r} + \frac{1}{r}\frac{\partial \sigma_{r\theta}}{\partial \theta} + \frac{\sigma_{rr} - \sigma_{\theta\theta}}{r} = 0, \; \frac{\partial \sigma_{12}}{\partial x_1} + \frac{\partial \sigma_{22}}{\partial x_2} = 0 \quad or \quad \frac{\partial \sigma_{r\theta}}{\partial r} + \frac{1}{r}\frac{\partial \sigma_{\theta\theta}}{\partial \theta} + \frac{2\sigma_{r\theta}}{r} = 0 \tag{4.9}$$

Equations (4.9) are fulfilled automatically if σ_{11}, σ_{22} and σ_{12} expressed in terms of a stress function ψ (the Airy stress function) as

$$\sigma_{11} = \frac{\partial^2 \psi}{\partial x_2^2} \quad or \; \sigma_{rr} = \frac{1}{r}\frac{\partial \psi}{\partial r} + \frac{1}{r^2}\frac{\partial^2 \psi}{\partial \theta^2}, \; \sigma_{22} = \frac{\partial^2 \psi}{\partial x_1^2} \; or \; \sigma_{\theta\theta} = \frac{\partial^2 \psi}{\partial r^2}, \sigma_{12} = -\frac{\partial^2 \psi}{\partial x_1 x_2} \; or \; \sigma_{r\theta} = -\frac{\partial}{\partial r}\frac{\partial \psi}{r \partial \theta} \tag{4.10}$$

5. FORMULATION OF PROBLEM

5.1 Single Edge Dislocation/Circular Phase Interaction

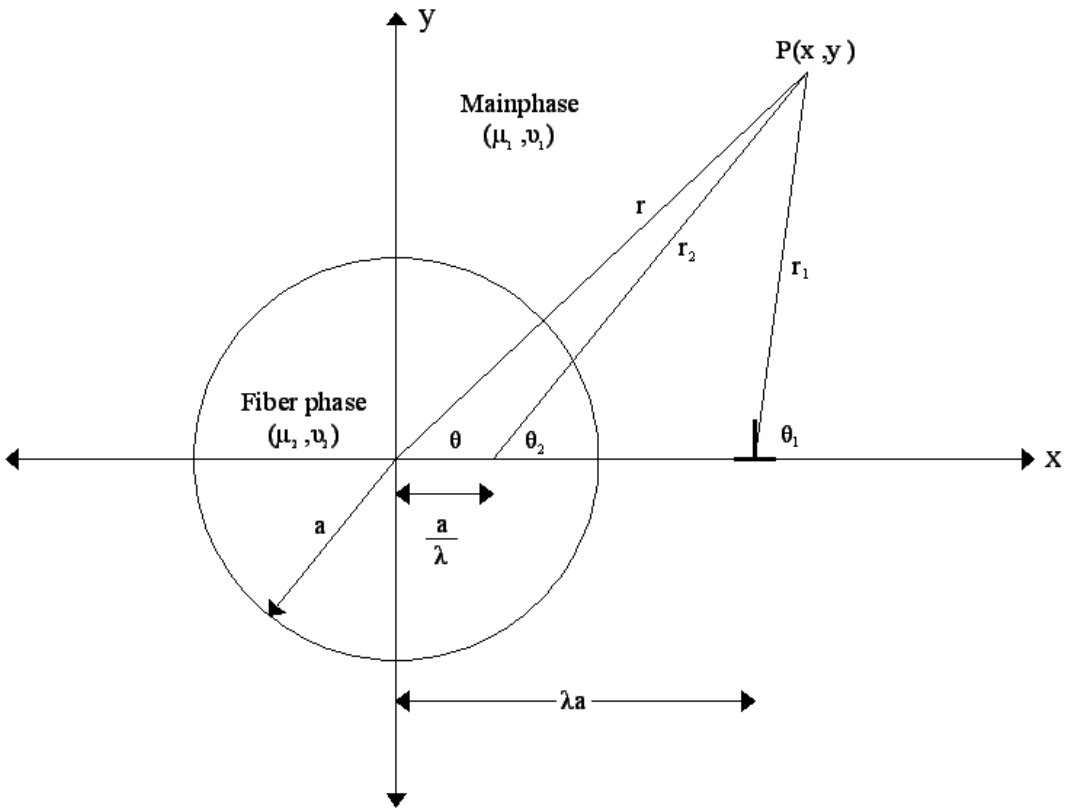

Figure 5.1: Single edge dislocation against a circular/cylindrical interface

$$\varphi^a = -\frac{2\mu_1 b}{\pi(K_1+1)}\left\{r_1 \ln r_1 \sin\theta_1 + C_1(r_2 \ln r_2 \sin\theta_2 - r \ln r \sin\theta) + C_2\left(r_2\theta_2 \cos\theta_2 - r\theta\cos\theta + \frac{a}{\lambda}\theta\right) - C_3\left[\frac{(\lambda^2-1)a}{\lambda^3}\left(\sin 2\theta_2 - \frac{(\lambda^2-1)a}{\lambda}\frac{\sin\theta_2}{r_2}\right) + a^2\frac{\sin\theta}{r}\right]\right\} \quad \textbf{(5.1)}$$

$$K_1 = 3 - \upsilon_1 \quad \textbf{(5.2)}$$

Let us rewrite φ^a in cartesian coordinates.

It can be seen in geometry of Figure 5.1 that we can write down following equations;

$$x = r\cos\theta \quad y = r\sin\theta \quad r_2 = \left[\left(x - \frac{a}{\lambda}\right)^2 + y^2\right]^{1/2} \tag{5.3.a}$$

$$x - \frac{a}{\lambda} = r_2 cos\theta \quad y = r_2 sin\theta_2 \quad r_2 = [(x - \lambda a)^2 + y^2]^{1/2} \tag{5.3.b}$$

$$x - \lambda a = r_1 cos\theta \qquad y = r_1 sin\theta_1 \qquad r = (x^2 + y^2)^{1/2} \tag{5.3.c}$$

We can also rewrite θ, θ_1 and θ_2 from Figure 5.1

$$\theta = atan\left({}^{y}/_{x}\right) \qquad \theta_1 = atan\left({}^{y}/_{(x - \lambda a)}\right) \qquad \theta_2 = \left({}^{y}\Big/_{\left(x - {}^{a}/_{\lambda}\right)}\right) \tag{5.4}$$

φ^a is very long function. So we can sperate it in four different subfunctions;

$$\varphi^a = f(\emptyset_1, \emptyset_2, \emptyset_3, \emptyset_4) \tag{5.5}$$

$$\emptyset_1 = r_1 ln r_1 sin\theta_1 = y ln r_1 = \frac{1}{2} y ln[(x - \lambda a)^2 + y^2] \tag{5.6.a}$$

$$\emptyset_2 = C_1(r_2\, ln\, r_2\, sin\, \theta_2 - r\, ln\, r\, sin\, \theta) = \frac{1}{2} C_1 y ln\left[\frac{\left(x - {}^{a}/_{\lambda}\right)^2 + y^2}{(x^2 + y^2)}\right] \tag{5.6.b}$$

$$\emptyset_3 = C_2\left(r_2\theta_2\, cos\, \theta_2 - r\theta\, cos\, \theta + \frac{a}{\lambda}\theta\right) = C_2\left[\left(x - {}^{a}/_{\lambda}\right)\left[atan\left({}^{y}/_{(x - \lambda a)}\right) - atan\left({}^{y}/_{x}\right)\right]\right] \tag{5.6.c}$$

$$\emptyset_4 = C_3\left[\frac{(\lambda^2 - 1)a}{\lambda^3}\left(sin\, 2\theta_2 - \frac{(\lambda^2 - 1)a}{\lambda}\frac{sin\, \theta_2}{r_2}\right) + a^2\frac{sin\, \theta}{r}\right] =$$

$$C_3\left[\frac{(\lambda^2 + 1)a}{\lambda^3}\left[\frac{y\left(x - {}^{a}/_{\lambda}\right)}{\left(\left(x - {}^{a}/_{\lambda}\right)^2 + y^2\right)^{3/2}} - \frac{(\lambda^2 + 1)a}{\lambda}\frac{y}{\left(x - {}^{a}/_{\lambda}\right)^2 + y^2}\right] + \frac{a^2 y}{x^2 + y^2}\right] \tag{5.6.d}$$

We can substitute $\emptyset_1, \emptyset_2, \emptyset_3, \emptyset_4$ in eq. 5.5, so that airy function will be written;

$$\varphi^a = -\frac{2\mu_1 b}{\pi(K_1 + 1)}(\emptyset_1 + \emptyset_2 + \emptyset_3 - \emptyset_4) \tag{5.7}$$

σ_{xy} will be calculated in cartesian coordinates, so we need to write φ^a function in cartesian coordinates.

From 5.7 and eq. 5.6.a, 5.6.b, 5.6,c φ^a can written as following;

$$\varphi^a = -\frac{2\mu_1 b}{\pi(K_1+1)}\left\{\frac{1}{2}yln[(x-\lambda a)^2+y^2]+\frac{1}{2}C_1 yln\left[\frac{\left(x-a/\lambda\right)^2+y^2}{(x^2+y^2)}\right]+C_2\left[\left(x-a/\lambda\right)\left[atan\left(y/(x-\lambda a)\right)-atan(y/x)\right]\right]-C_3\left[\frac{(\lambda^2+1)a}{\lambda^3}\left[\frac{y\left(x-a/\lambda\right)}{\left(\left(x-a/\lambda\right)^2+y^2\right)^{3/2}}-\frac{(\lambda^2+1)a}{\lambda}\frac{y}{\left(x-a/\lambda\right)^2+y^2}\right]+\frac{a^2y}{x^2+y^2}\right]\right\} \quad \textbf{(5.8)}$$

Eq. 5.8 has been written in matlab m-file in symbolic toolbox. $\sigma_{rr}, \sigma_{\theta\theta}, \sigma_{r\theta}$ eq. 4.4 calculated.

5.2 Symbolic Math Toolbox

Symbolic Math Toolbox™ provides tools for solving and manipulating symbolic math expressions and performing variable-precision arithmetic. The toolbox contains hundreds of MATLAB® symbolic functions that advantage the MuPAD® engine for tasks such as differentiation, integration, simplification, transforms, and equation solving.

Symbolic Math Toolbox also includes the MuPAD language, which is optimized for handling and operating on symbolic math expressions. It provides libraries of MuPAD functions in common mathematical areas, such as calculus and linear algebra, as well as specialized areas, such as number theory and combinatory. You can extend the built-in functionality by writing custom symbolic functions and libraries in the MuPAD language.

All functions can be accessed from the MATLAB command line or from the MuPAD notebook interface, where you can manage and document your symbolic computations [43].

Single edge dislocation shear stress,

$$\sigma_{xy} = -\frac{\partial^2 \varphi^a}{\partial x \partial y} \quad \textbf{(5.9)}$$

Eq. 5.9 calculated in matlab symbolic toolbox

On glide pane $(\theta = 0,\ \ y = 0)$;

$$\sigma_{xy}(x \geq a,\ \ y = 0) = \sigma_{r\theta}(r \geq a,\ \ \theta = 0)$$

$$\sigma_{r\theta}(r \geq a,\ \ \theta = 0) = -\frac{2\mu_1 b}{\pi(K_1+1)}\left\{\frac{1}{r-\lambda a} + C_1\left(\frac{1}{r-\frac{a}{\lambda}} - \frac{1}{\lambda}\right) - C_2\frac{a}{\lambda r^2} + 2C_3\left[\frac{(\lambda^2-1)a}{\lambda^3\left(r-\frac{a}{\lambda}\right)^2} - \frac{(\lambda^2-1)^2 a}{\lambda^4\left(r-\frac{a}{\lambda}\right)^3} + \frac{2a^2}{r^3}\right]\right\} \quad \textbf{(5.10)}$$

Eq. 5.10 calculated in imatlab symbolic toolbox.

6. COMPUTATIONAL PROCEDURE

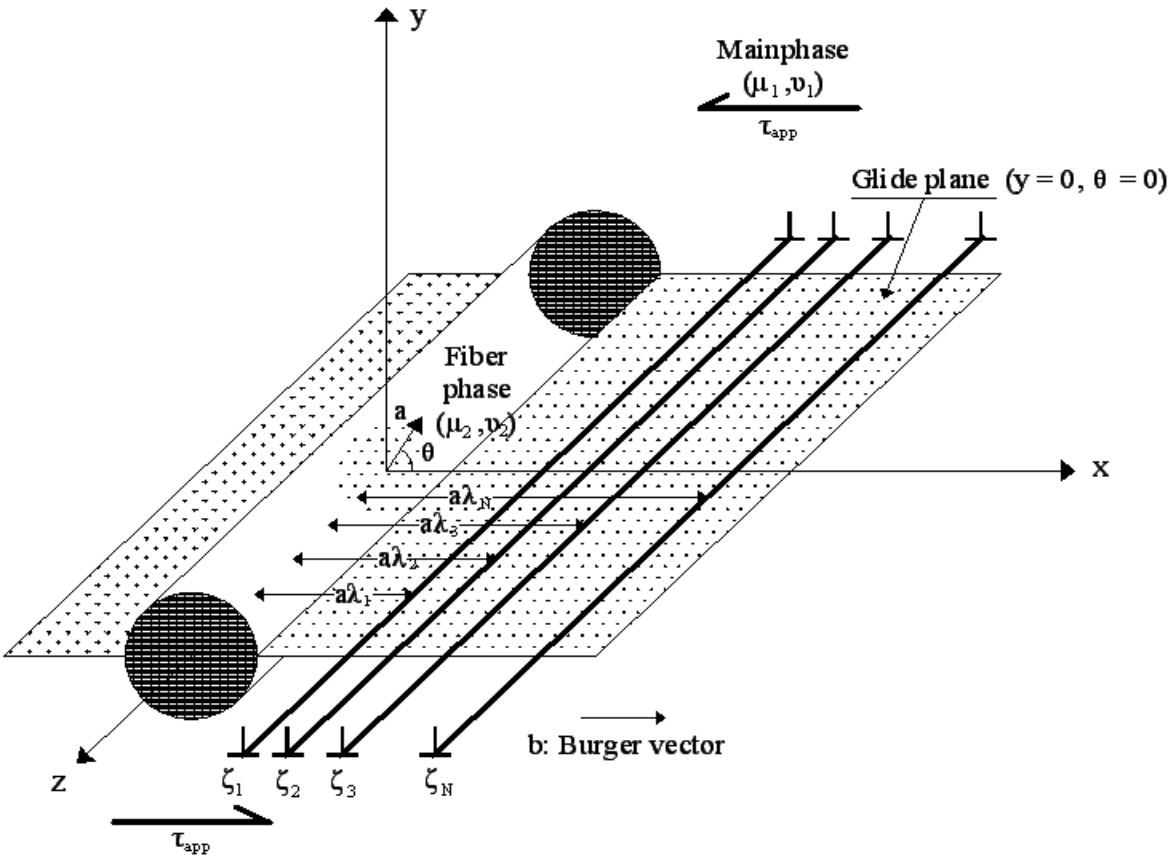

Figure 6.1: The Multiple edge dislocation pile-up against a circular/cylindrical interface [44].

In static equilibrium conditions shcmid shear strain and strain created by dislocation;

$$\tau_{app} = -\sigma_{r\theta}(r \geq a,\ \theta = 0) \qquad \textbf{(6.1)}$$

In this case, the leading dislocation never reaches the interface as illustrated schematically in Fig. 6.1 [5].

The condition that the equilibrium array configuration corresponds to zero Peach-Koehler force on each array dislocation is equivalent to requiring that at each of the N dislocations, the finite part of the total glide plane shear stress given by the sum of the equation (5.10) and (6.1).

The equilibrium dislocation positions must be obtained by solving N nonlinear algebraic equations, namely;

$$\sum_{\substack{n=1 \\ n\neq m}}^{N} \frac{1}{\lambda_m-\lambda_n} - C_1\left(\frac{1}{\lambda_m} - \sum_{n=1}^{N}\frac{\lambda_n}{\lambda_m\lambda_n-1}\right) - C_2\sum_{n=1}^{N}\frac{1}{\lambda_n\lambda_m^2} + 2C_3\left(\sum_{n=1}^{N}\frac{\lambda_n^2-1}{\lambda_n(\lambda_m\lambda_n-1)^2} - \sum_{n=1}^{N}\frac{(\lambda_n^2-1)^2}{\lambda_n(\lambda_m\lambda_n-1)^3}\right) + \frac{2C_3}{\lambda_m^3} = \frac{a\pi(K_1+1)\tau_{app}}{2\mu_1 b} = R \quad \textbf{(6.2)}$$

Equation (6.2) represents N nonlinear algebraic equations for each N unknown which must be solved numerically.

6.1 Numerical Method

6.1.1 Optimization Overview

In mathematics and computer science, an optimization problem is the problem of finding the best solution from all feasible solutions. Optimization is a solution of an equation or we can say that it is the optimal value of a root of an equation. Optimization is very essential for engineering problems. Most of complex engineering problems can be designed or solved by optimization techniques. Optimization techniques are used to find a set of design parameters, $= \{x_1, x_2, \dots, x_n\}$, that can in some way be defined as optimal [45]. In a simple case this might be the minimization or maximization of some system characteristic that is dependent on x. In a more advanced formulation the objective function, f(x), to be minimized or maximized, might be subject to constraints in the form of equality constraints, or unconstrained. Optimization problems can be classified in two general cases, constrained and unconstrained optimizations.

6.1.1.1 Constrained Optimization problem

An optimization or a mathematical programming problem can be stated as follows

$$\text{Find } X = \begin{Bmatrix} x_1 \\ x_2 \\ x_3 \\ \cdot \\ \cdot \\ \cdot \\ x_n \end{Bmatrix} \text{ which minimize } f(x)$$

Subject to the constraints

$$\left\{\begin{matrix} g_j(x) \leq 0, & j = 1, 2, \dots\dots, m \\ I_j(x) \leq 0, & j = 1, 2, \dots\dots, p \end{matrix}\right\} \quad \textbf{(6.3)}$$

Where X is an n-dimensional vector called the design vector, $f(x)$ is termed the objective function, and $g_j(x)$ and $I_j(x)$ are known as inequality and equality constraints, respectively. The number of variables *n* and the number of constraints *m* and/or/p need not be related in any way. The problem stated in Equations (6.3) is called a constrained optimization problem [46].

6.1.1.2 Unconstrained Optimization problem

An unconstrained problem is a problem of the form to minimize $f(x)$ without any constraints on the vector x. Unconstrained problems seldom arise in practical applications [47]. In this study, the optimization procedure will be solving by unconstrained optimization technique.

$$\text{Find } X = \begin{Bmatrix} x_1 \\ x_2 \\ x_3 \\ \cdot \\ \cdot \\ \cdot \\ x_n \end{Bmatrix} \text{ which minimize } f(x) \quad \textbf{(6.4)}$$

The problem stated in equation (6.4) called unconstrained optimization problem.
It is true that rarely a practical design problem would be unconstrained; still, a study of this class of problems is important for the following reasons [46]:

- The constraints do not have significant influence in certain design problems.
- Some of the powerful and robust methods of solving constrained minimization problems require the use of unconstrained minimization techniques.
- The study of unconstrained minimization techniques provide the basic understanding necessary for the study of constrained minimization methods.
- The unconstrained minimization methods can be used to solve certain complex engineering analysis problems.

6.2 Optimization Toolbox

Optimization Toolbox extends the MATLAB® technical computing environment with tools and widely used algorithms for standard and large-scale optimization. These algorithms solve constrained and unconstrained continuous and discrete problems. The toolbox includes functions for linear programming, quadratic programming, nonlinear optimization, nonlinear least squares, solving systems of nonlinear equations, multi-objective optimization and binary integer programming [45].

This is a constrained optimization problem that solved in matlab optimization tool box. Constrained minimization is the problem of finding a minimum of a constrained nonlinear multivariable function$f(x)$ [45].

$\min_{x} f(x)$ Subject to

$c(x) \leq 0$

$ceq(x) = 0$

$A.x \leq b$

$Aeq.x = beq$

$lb \leq x \leq ub$

where x, b, beq, lb, and ub are vectors, A and Aeq are matrices, c(x) and ceq(x) are functions that return vectors, and f(x) is a function that returns a scalar. f(x), c(x), and ceq(x) can be nonlinear functions.

For $i = 1, 2, 3, \ldots\ldots, N$ equations and N unknowns, the aim is to find a solution vector $X = (X_1, X_2, \ldots., X_N)$, which minimize the objective function$f(x)$. In constrained optimization, the main aim is to divide the problem into an easier sub problem that can then be solved and used as the basis of an iterative process. A characteristic of a large class of early methods is the translation of the constrained problem to a basic unconstrained problem by using a penalty function for constraints that are near or beyond the constraint boundary [48]. In this way, the constrained problem is solved using a sequence of parameterized unconstrained optimizations, which in the limit (of the sequence) converge to the constrained problem.

6.2.1 Large Scale Fmincon Algorithm

6.2.1.1 Trust-Region Methods for Nonlinear Minimization

Many of the methods used in Optimization Toolbox solvers are based on trust regions, a simple yet powerful concept in optimization [49]. The unconstrained minimization problem does not have any constrains, so there must be some restriction to find minimum $f(x)$ in any x points, here x is a vector. For any function in a point x in *n*-space when the function move to a point with a lower function value, in this case a lower function value means that the objective function will be in a lower direction. The basic idea is to approximate f with a simpler function q, which reasonably reflects the behavior of function f in a neighborhood N around the point x. This neighborhood is the trust region [49]. A trial step s is computed by minimizing (or approximately minimizing) over *N*. This is the trust-region sub problem [49],

$$\min_{s}\{q(s), s \in N\}$$

The current point is updated to be x + s if f(x + s) < f(x); otherwise, the current point remains unchanged and *N*, the region of trust, is shrunk and the trial step computation is repeated.

The key questions in defining a specific trust-region approach to minimizing f(x) are how to choose and compute the approximation q (defined at the current point x), how to choose and modify the trust region *N*, and how accurately to solve the trust-region sub problem. In the standard trust-region method [50], the quadratic approximation q is defined by the first two terms of the Taylor approximation to F at *x*; the neighborhood N is usually spherical or ellipsoidal in shape. Mathematically the trust-region sub problem is typically stated [49].

$$min\left\{\frac{1}{2}s^T Hs + s^T \; such\; that \; \|D_s\| \leq \Delta\right\} \qquad \textbf{(6.5)}$$

Where g is the gradient of f at the current point x, H is the Hessian matrix (the symmetric matrix of second derivatives), D is a diagonal scaling matrix, Δ is a positive scalar, and ‖ . ‖ is the 2-norm.

Such algorithms provide an accurate solution to equation (6.5) However, they require time proportional to several factorizations of H. Therefore, for large-scale problems a different approach is needed. Once the subspace S has been computed, the work to solve equation (6.5) is trivial even if full eigenvalue/eigenvector information is needed. The dominant work has now shifted to the determination of the subspace [49]. The two-dimensional subspace S is determined with the aid of a preconditioned conjugate gradient process described below. The solver defines S as the linear space spanned by s_1 and s_2, where s_1 is in the direction of the gradient g, and s_2 is either an approximate Newton direction, i.e., a solution to

$$H.s_2 = -g$$

Or a direction of negative curvature

$$s_2^T.H.s_2 < 0$$

The philosophy behind this choice of S is to force global convergence (via the steepest descent direction or negative curvature direction) and achieve fast local convergence (via the Newton step, when it exists).

A sketch of unconstrained minimization using trust-region ideas is now easy to give:

- Formulate the two-dimensional trust-region sub problem.
- Solve equation (6.5) to determine the trial step s.
- $if\ f(x+s) < f(x), then\ x = x + s$
- Adjust Δ

These four steps are repeated until convergence. The trust-region dimension Δ is adjusted according to standard rules. In particular, it is decreased if the trial step is not accepted, i.e., $f(x+s) \geq f$ [51] and [52].

6.2.1.2 Nonlinear Minimization with Gradient and Hessian

Equation (6.2) a nonlinear minimization problem with a tridiagonal Hessian matrix H(x) first computed explicitly, and then by providing the Hessian's sparsity structure for the finite-differencing routine. The problem is to find x to minimize $f(x)$,

Where $x_n = \lambda_n, x_m = \lambda_m$ equation (6.2) can be written in following form for optimization

$$f(x) =$$

$$\sum_{\substack{n=1 \\ n\neq m}}^{N} \frac{1}{x_m - x_n} - C_1\left(\frac{1}{x_m} - \sum_{n=1}^{N} \frac{x_n}{x_m x_n - 1}\right) - C_2 \sum_{n=1}^{N} \frac{1}{x_n x_m^2} + 2C_3\left(\sum_{n=1}^{N} \frac{x_n^2 - 1}{x_n (x_m x_n - 1)^2} - \sum_{n=1}^{N} \frac{(x_n^2 - 1)^2}{x_n (x_m x_n - 1)^3}\right) + \frac{2C_3}{x_m^3} - \frac{a\pi(K_1+1)\tau_{app}}{2\mu_1 b} = 0 \quad \textbf{(6.6)}$$

$$R = \frac{a}{D} \quad \text{where } D = \frac{2\mu_1 b}{\pi(K_1+1)\tau_{app}} \quad \textbf{(6.7)}$$

$$X_n = \frac{x_n}{D} = R(\lambda_n - 1); \quad n = 1, 2, \ldots, N \quad \textbf{(6.8)}$$

$$m = 1, 2, \ldots, N$$

$$C_1, C_2, C_3 = f(\mu_1, \mu_2, v_1, v_2)$$

7. RESULTS AND DISCUSSION

7.1 General optimization

An M-file symbolic.m was written that computes objective function in symbolic toolbox and symbolic_hessian.m was written that computes the hessian, gradient of the objective function in symbolic toolbox. The output of this M-file consists of only symbolics characters. These M-file was used in tezfgHessian.m for easy calculate hessian and gradient of objective function. Finally, the objective function was called by generaloptimization.m file. The values listed in Table 7.1 for $\Gamma = 3.00$, $\upsilon_1 = \upsilon_2 = 0.33$ has been predicted by optimization process. Numerical optimization has been done for 30 dislocations. Fort this pile-up dislocation system, 30 different nonlinear function had been optimized. For i = 1, 2 …N equations and N unknowns, the aim is to find a solution vector X= (X_1, X_2… X_N) which optimized a defined function. Therefore, 30 nonlinear system of equation has been optimized. The results listed in Table 7.1

Table 7.1: Dimensionless standoff distances of edge dislocations against a circular/cylindrical interface in units of x/D for the condition $\Gamma = 3.00$, $\upsilon 1 = \upsilon 2 = 0.33$.

n	X_1	X_2	X_3	X_4	X_5		X_{10}		X_{20}		X_{30}
1	1,0548	-	-	-	-	.....	-	.....	-	.....	-
2	0,96668	1,3819	-	-	-	.....	-	.....	-	.....	-
3	0,87293	1,2718	1,825	-	-	.....	-	.....	-	.....	-
4	0,69526	1,0324	1,5316	2,3362	-	.....	-	.....	-	.....	-
5	0,65443	0,94343	1,4146	2,1129	2,8877	.....	-	.....	-	.....	-
⋮	⋮										
10	0,29149	0,43728	0,66371	0,99647	1,4951	.....	7,2343	.....	-	.....	-
⋮	⋮										
20	0,13461	0,1864	0,28183	0,45508	0,69867	....	3,3899	.....	20,584	.....	-
⋮	⋮										
30	0,056151	0,07949	0,11921	0,3014	0,51503	.....	2,5214	.....	15,38	.....	75,75

The mathematical formulation of the dislocation pile-up problem may allow understanding two important aspects of structure/property relationships in particle-strengthened materials [5].

First, it is possible to investigate the effects of changing the resolved applied shear stress by varying τ_{app}/μ_1. Secondly, it is possible to study the effects of microstructure, history and thermo mechanical conditions by varying Λ=L/b, the dimensionless pile-up length. The shear stress values at the tip of the active slip plane for each case are to be evaluated in assessing each case. In addition, it is possible to apply mathematical modeling results for three different composite materials and compare the results for those two important cases.

7.1.1 Effect of varying τ_{app}/μ_1

Figure 7.1. shows the variation of tip shear stress $S_{r\theta}(r = a, \theta = 0)$ as a function of the dimensionless applied or resolved shear stres, τ_{app}/μ_1, for the different in homogeneity types (Γ =1.5, Γ = 2.20, Γ = 3.00). Figure 7.1. shows the discrete nature of dislocation arrays in a pile-up for a constant pile-up length. For constant value of Γ poison ratios and dimensionless length Λ, the discrete values of dimensionless applied stress, τ_{app}/μ_1, can be calculated by using equation (6.7) and equation (6.8)

$$\left(\frac{\tau_{app}}{\mu_1}\right) = \frac{2}{\pi(K_1+1)}\frac{1}{\Lambda}X_i, \qquad i = 1,2,3,\ldots,N \tag{7.1}$$

Where X_i is the dimensionless standoff distance of the ith dislocation in an array of i dislocations and $(\tau_{app}/\mu_1)_i$ is the lower bound of dimensionless applied stress for an array of i dislocations when Λ is a constant. According to Figure 7.1. The size of discontinuity, the change in the tip shear stress when another dislocation is introduced, is larger for elastically harder material than for a weaker one. As a result, the roll up of a given shear stress at the cylindrical fiber interface needs a smaller resolved shear stress for a weaker fiber.

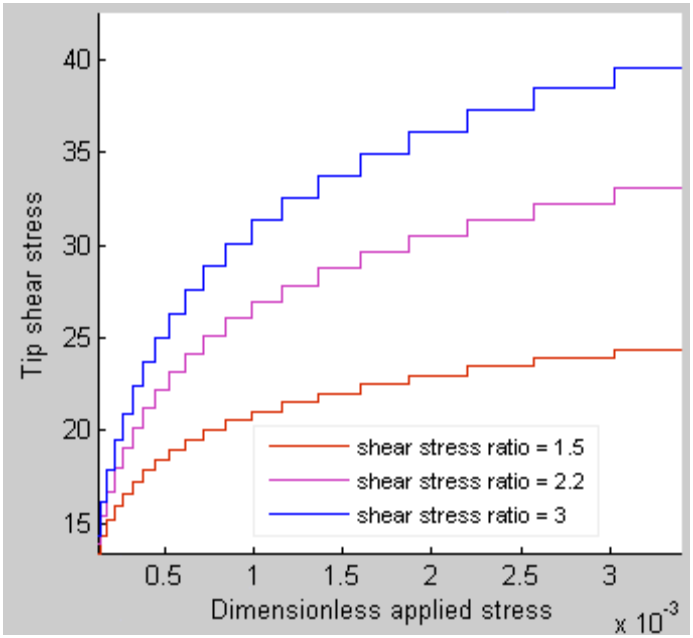

Figure 7.1: Variation of tip stress, S_0, as a function of the applied stres, τ_{app}/μ_1, for the second phase (fiber phase) is elastically harder than the matrix ($\Gamma>1$) at constant dimensionless pile-up lengths and poison ratios, $\upsilon_1 = \upsilon_2 = 0.33$.

7.1.2 Effect of changing microstructure, varying Λ

Figure 7.2 shows the variation of tip shear stres $S_{r\theta}(r = a, \theta = 0)$ as a function of the dimensionless pile-up length, Λ, for different stresses and at constant Γ, υ_1, υ_2. The discrete, discontinuous for different applied stress values, τ_{app}/μ_1, shows that the discrete nature of the dislocations in a pile-up. For a constant shear stres ratio, Γ= 2.2, a critical value of Λ can be defined which there would not be any dislocation. When the defined critical value of Λ exceeded, then one dislocation is introduced into the pile-up, and contribution to the tip shear stress will include the stress field of dislocation. From figure 7.2 when Λ increased more and more, more and more dislocations are allow in and each of contributes to the local stres buildup in a discontinuity way will be a result of a discontinuity at values of Λ pertaining to a different number of dislocations [5]. For constant values Γ=2.20, $\upsilon_1 = \upsilon_2 = 0.33$ and constant dimensionless applied stress τ_{app}/μ_1, the discrete values of dimensionless pile-up length, Λ, were calculated by using equation (6.7) and equation (6.8)

$$\Lambda_i = \frac{2}{\pi(K_1+1)}\frac{\mu_1}{\tau_{app}}X_i, \qquad i = 1,2,3,\dots,N \tag{7.2}$$

Where X_i is the dimensionless standoff distance of the ith dislocation in an array of i dislocations and, Λ_i is the lower bound of dimensionless pile-up length for an array of i dislocations at constant τ_{app}/μ_1. The maximum value of the dimensionless pile-up length for an array of *i* dislocations is supposed to be equal to that of the minimum value for $i + 1$ dislocations. We can say that when τ_{app}/μ_1 increased the critical dimensionless plie-up length is decreasing in Figure 7.2. Increasing τ_{app}/μ_1, does not affect the dimensionless standoff values, since the solution is a function only of the composite variables, but increases N that can be seen as an increasing number of steps in the discrete representation. Thus, the S vs Λ curves shift to higher values for increasing τ_{app}/μ_1. Therefore, a larger stress is needed to start plastic deformation for smaller pile-up lengths.

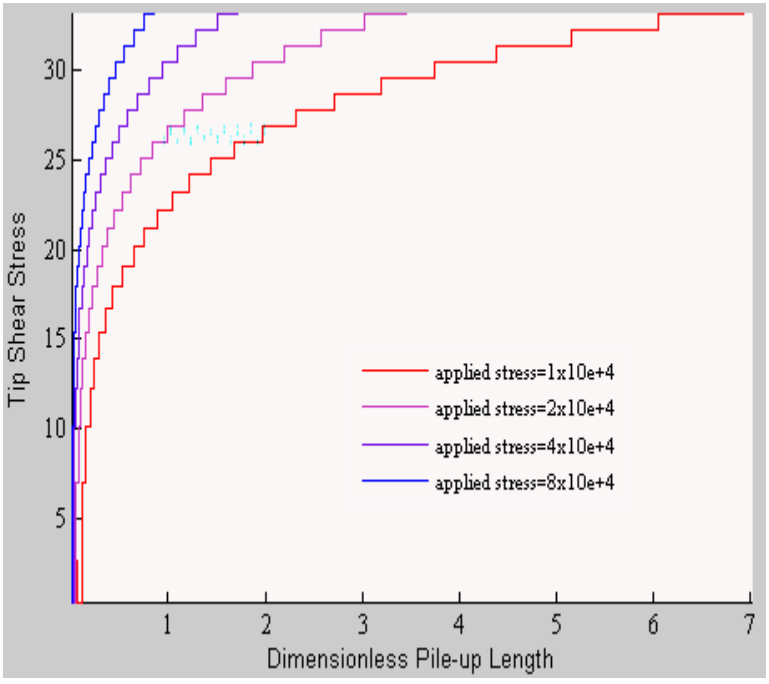

Figure 7.2: Variation of the tip stres, S_0, as a function of dimensionless pile-up length, Λ, for Γ=2.20 and at constant poison ratioes, $\upsilon_1 = \upsilon_2 = 0.33$.

7.2 Application of Results for Three Special Cases

7.2.1 Al/Al_2O_3

All numerical processes applied for Al/Al_2O_3 special case. The input values were taken from Table 7.2. Firstly, a system of nonlinear equation was solved for given values. For i = 1, 2 …N equations and N unknowns, the aim is to find a solution vector X= (X_1, X_2… X_N) which optimized a defined function. Therefore, 30 nonlinear system of equation has been optimized. The results are listed in Table 7.3. The effects of changing the resolved applied shear stress by varying τ_{app}/μ_1 and the effects of microstructure, history and thermomechanical conditions by varying Λ=L/b, the dimensionless pile-up length was investigated for Al/Al_2O_3 case.

Table 7.2: Mechanical properties of Al, Cu, SiC, WC, Al_2O_3 [53, 54 and 55]

Material	Elsatic Module	Shear Module	Poison Ratio
Aluminum [Al]	70 Gpa	26 Mpa	0.33
Copper [Cu]	110 - 120 Gpa	40 - 47 Mpa	0.33 - 0.36
Silicon Carbide [SiC]	-	179(3%) Mpa	0.16(25%)
Wolfram Carbide [WC]	668.35 .. 713.82 GPa	269,35 Mpa	0,24
Aumina(Al_2O_3)	372,54 Gpa	152,22 Mpa	0,22

Table 7.3: Dimensionless standoff distances of edge dislocations against a circular/cylindrical interface in units of x/D for the condition $\Gamma = 5.85$, $\upsilon_1 = 0.33$ $\upsilon_2 = 0.22$

n	X_1	X_2	X_3	X_4	X_5	....	X_{10}	.....	X_{20}	.....	X_{30}
1	1,0713	-	-	-	-	.....	-	.....	-	.....	-
2	0,92816	1,4538	-	-	-	.....	-	.....	-	.....	-
3	0,86673	1,2729	1,9027	-	-	.....	-	.....	-	.....	-
4	0,68295	1,0498	1,5926	2,4961	-	.....	-	.....	-	.....	-
5	0,5521	0,95472	1,4559	2,1693	3,2517	.....	-	.....	-	.....	-
⋮	⋮	⋮	⋮	⋮	⋮						
10	0,28828	0,48711	0,67986	1,058	1,62	.....	6,723	.....	-	.....	-
⋮	⋮	⋮	⋮	⋮	⋮		⋮				
20	0,12934	0,20558	0,31359	0,49325	0,75659	....	3,1146	.....	19,831	.....	-
⋮	⋮	⋮	⋮	⋮	⋮		⋮		⋮		
30	0,055514	0,085179	0,1287	0,33311	0,5591	.....	2,317	.....	14,748	.....	85,234

7.2.1.1 Effect of varying τ_{app}/μ_1

Figure 7.3 shows the variation of tip shear stress $S_{r\theta}(r = a, \theta = 0)$ as a function of the dimensionless applied or resolved shear stres, τ_{app}/μ_1, for the different in homogeneity types (Γ = 5.85, υ_1 = 0.33 υ_2 = 0.22 Table 7.2) Figure 7.3 shows the discrete nature of dislocation arrays in a pile-up for a constant pile-up length. For constant value of Γ poison ratios and dimensionless length Λ, the discrete values of dimensionless applied stress, τ_{app}/μ_1, can be calculated by using equation (7.1)

According to Figure 7.3 the size of discontinuity, the change in the tip shear stress when another dislocation is introduced, is lower when dimensionless applied stress increases. As a result, the roll up of a given shear stress at the cylindrical fiber interface needs a high resolved shear stress for a Al_2O_3 fiber. Al_2O_3 is elastically harder than Al, so the obtained results from Figure 7.3 are satisfied by the general optimization results.

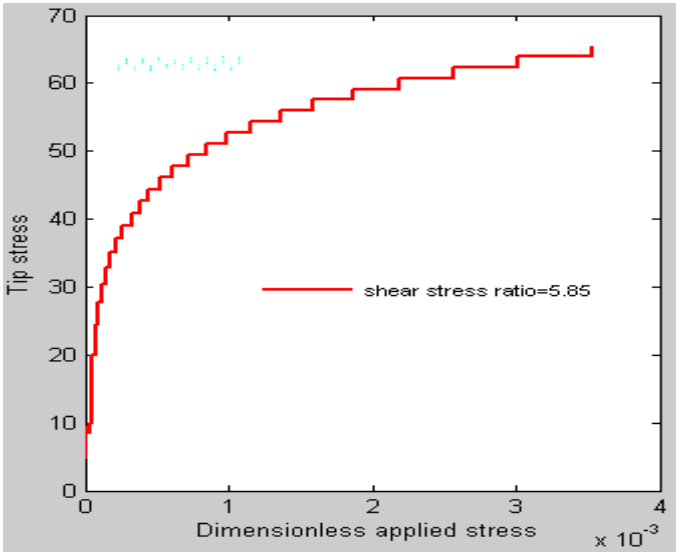

Figure 7.3: Variation of tip stress, S_0, as a function of the applied stres, τ_{app}/μ_1, for the Al_2O_3 phase (fiber phase) is elastically harder than the matrix (Γ>1) at constant dimensionless pile-up lengths and poison ratios, υ_1 = 0.33 υ_2 = 0.22.

7.2.1.2 Effect of changing microstructure, varying Λ

Figure 7.4 shows the variation of tip shear stres $S_{r\theta}(r = a, \theta = 0)$ as a function of the dimensionless pile-up length, Λ, for different stresses and at constant Γ, υ_1, υ_2. The discrete, discontinuous for different applied stress values, τ_{app}/μ_1, shows that the discrete nature of the dislocations in a pile-up. For a constant shear stres ratio, Γ =

5.85. A critical value of Λ can be defined which there would not be any dislocation. When the defined critical value of Λ exceeded, then one dislocation is introduced into the pile-up, and contribution to the tip shear stress will include the stress field of dislocation. From figure 7.3 when Λ increased more and more, more and more dislocations are allow in and each of contributes to the local stres buildup in a discontinuity way will be a result of a discontinuity at values of Λ pertaining to a different number of dislocations [5]. For constant values $\Gamma = 5.85$, $\upsilon_1 = 0.33$ $\upsilon_2 = 0.22$ and constant dimensionless applied stress τ_{app}/μ_1, the discrete values of dimensionless pile-up length, Λ, were calculated by using equation (7.2)

The maximum value of the dimensionless pile-up length for an array of *i* dislocations is supposed to be equal to that of the minimum value for $i + 1$ dislocations. We can say that when τ_{app}/μ_1 increased the critical dimensionless plie-up length is decreasing in Figure 7.4. Increasing τ_{app}/μ_1, does not affect the dimensionless standoff values, since the solution is a function only of the composite variables, but increases N that can be seen as an increasing number of steps in the discrete representation. Thus, the S vs Λ curves shift to higher values for increasing τ_{app}/μ_1. Therefore, a larger stress is needed to start plastic deformation for smaller pile-up lengths. As a result of comparation of Figure 7.2 and Figure 7.4, we can say that when fiber is elestically harder the varying in tip shear stress increases.

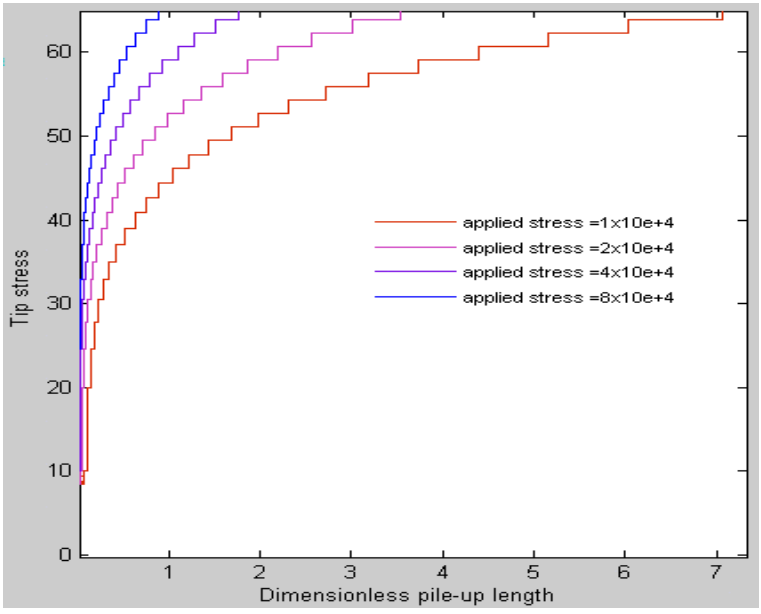

Figure 7.4: Variation of the tip stres, S_0, as a function of dimensionless pile-up length, Λ, for $\Gamma = 5.85$, $\upsilon_1 = 0.33$ $\upsilon_2 = 0.22$.

7.2.2 Cu/WC

All numerical processes applied for Cu/WC special case. The input values was taken from Table 7.2. Firstly, a system of nonlinear equation was solved for given values. For i = 1, 2 …N equations and N unknowns, the aim is to find a solution vector X= (X_1, X_2… X_N) which optimized a defined function. Therefore, 30 nonlinear system of equation has been optimized. The results are listed in Table 7.4. The effects of changing the resolved applied shear stress by varying τ_{app}/μ_1 and the effects of microstructure, history and thermomechanical conditions by varying Λ=L/b, the dimensionless pile-up length will be investigate for Cu/WC case.

Table 7.4: Dimensionless standoff distances of edge dislocations against a circular/cylindrical interface in units of x/D for the condition Γ = 6, υ_1 = 0.33 υ_2 = 0.24

n	X_1	X_2	X_3	X_4	X_5	....	X_{10}	.....	X_{20}	.....	X_{30}
1	1,0728	-	-	-	-	.....	-	.....	-	.....	-
2	0,98202	1,4351	-	-	-	.....	-	.....	-	.....	-
3	0,86531	1,255	1,9028	-	-	.....	-	.....	-	.....	-
4	0,67468	1,0489	1,5849	2,5181	-	.....	-	.....	-	.....	-
5	0,55721	0,95415	1,4582	2,172	3,2475	.....	-	.....	-	.....	-
⋮	⋮	⋮	⋮	⋮	⋮			.....	-	.....	-
10	0,28963	0,48685	0,67962	1,058	1,6201	.....	7,9809	.....	-	.....	-
⋮	⋮	⋮	⋮	⋮	⋮		⋮	.....	-	.....	-
20	0,13074	0,19864	0,29363	0,49018	0,75636	.....	3,8125	.....	23,213	.....	-
⋮	⋮	⋮	⋮	⋮	⋮		⋮		⋮	.....	-
30	0,055766	0,085342	0,12291	0,33138	0,55891	.....	2,8359	.....	17,3	.....	85,231

7.2.2.1 Effect of varying τ_{app}/μ_1

Figure 7.5 shows the variation of tip shear stres $S_{r\theta}(r = a, \theta = 0)$ as a function of the dimensionless applied or resolved shear stres, τ_{app}/μ_1, for the different in homogeneity types (Γ = 6, υ_1 = 0.33 υ_2 = 0.24 Table 7.2) Figure 7.5 shows the discrete nature of dislocation arrays in a pile-up for a constant pile-up length. For constant value of Γ poison ratioes and dimensionless length Λ, the discrete values of dimensionless applied stres, τ_{app}/μ_1, can be calculated by using equation (7.1)

According to Figure 7.5 the size of discontinuty, the change in the tip shear stress when another dislocation is introduced, is lower when dimensionless applied stres increases. As a result, the roll up of a given shear stress at the cylindirical fiber interface needs a high resolved shear stres for a WC fiber. WC is elastically harder than Al, so the obtained results from Figure 7.5 are satisfied by the general optimization results.

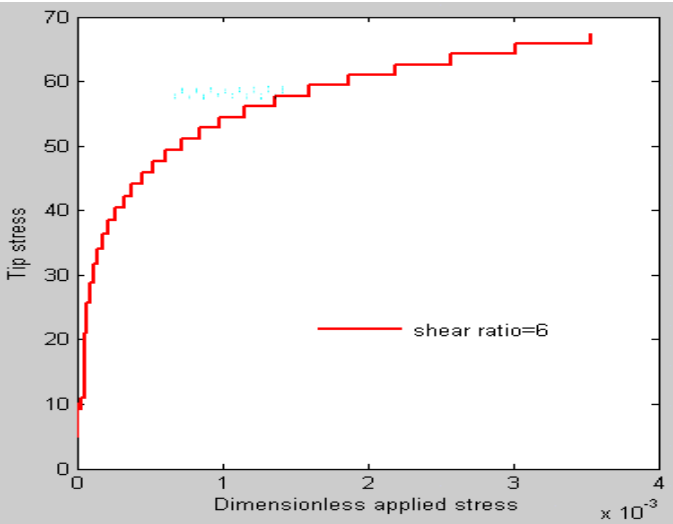

Figure 7.5: Variation of tip stress, S_0, as a function of the applied stres, τ_{app}/μ_1, for the WC phase (fiber phase) is elastically harder than the matrix ($\Gamma>1$) at constant dimensionless pile-up lengths and poison ratios, $\upsilon_1 = 0.33$ $\upsilon_2 = 0.24$.

7.2.2.2 Effect of changing microstructure, varying Λ

Figure 7.6 shows the variation of tip shear stres $S_{r\theta}(r = a, \theta = 0)$ as a function of the dimensionless pile-up length, Λ, for different stresses and at constant Γ, υ_1, υ_2. The discrete, discontinuous for different applied stress values, τ_{app}/μ_1, shows that the discrete nature of the dislocations in a pile-up. For a constant shear stres ratio, Γ = 6. A critical value of Λ can be defined which there would not be any dislocation. When the defined critical value of Λ exceeded, then one dislocation is introduced into the pile-up, and contribution to the tip shear stress will include the stress field of dislocation. From figure 7.6 when Λ increased more and more, more and more dislocations are allow in and each of contributes to the local stres buildup in a discontinuity way will be a result of a discontinuity at values of Λ pertaining to a different number of dislocations [5]. For constant values Γ = 6, $\upsilon_1 = 0.33$ $\upsilon_2 = 0.24$ and constant dimensionless applied stress τ_{app}/μ_1, the discrete values of dimensionless pile-up length, Λ, were calculated by using equation (7.2).

The maximum value of the dimensionless pile-up length for an array of *i* dislocations is supposed to be equal to that of the minimum value for *i* + 1 dislocations. We can say that when τ_{app}/μ_1 increased the critical dimensionless plie-up length is decreasing in Figure 7.6. Increasing τ_{app}/μ_1, does not affect the dimensionless standoff values, since the solution is a function only of the composite

variables, but increases N that can be seen as an increasing number of steps in the discrete representation. Thus, the S vs Λ curves shift to higher values for increasing τ_{app}/μ_1. Therefore, a larger stress is needed to start plastic deformation for smaller pile-up lengths.

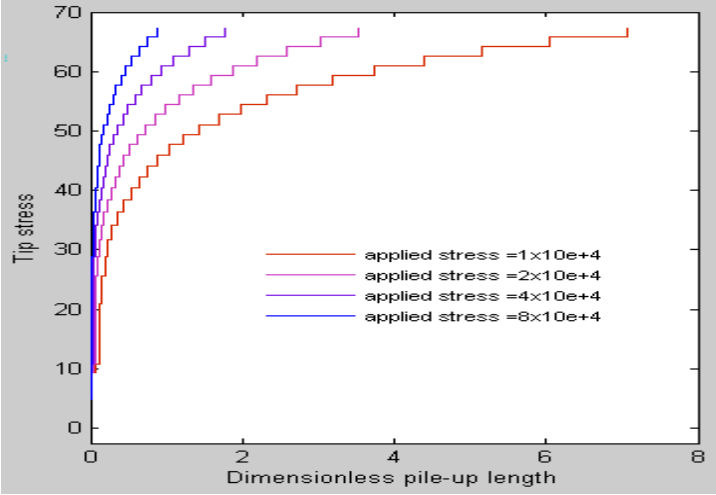

Figure 7.6: Variation of the tip stres, S_0, as a function of dimensionless pile-up length, Λ, for Γ = 6, υ_1 = 0.33 υ_2 = 0.24.

7.2.3 Al/SiC

All numerical processes applied for Al/SiC special case. The input values were taken from Table 7.2. Firstly, a system of nonlinear equation was solved for given values. For i = 1,2,……N equations and N unknowns, the aim is to find a solution vector X= (X_1, X_2, ….. X_N) which optimized a defined function. Therefore 30 nonlinear system of equation has been optimized. The results are listed in Table 7.5. The effects of changing the resolved applied shear stress by varying τ_{app}/μ_1 and the effects of microstructure, history and thermomechanical conditions by varying Λ=L/b, the dimensionless pile-up length will be investigate for Al/SiC case.

Table 7.5: Dimensionless standoff distances of edge dislocations against a circular/cylindrical interface in units of x/D for the condition Γ = 6.88, υ_1 = 0.33 υ_2 = 0.16

n	X_1	X_2	X_3	X_4	X_5	....	X_{10}	.....	X_{20}	.....	X_{30}
1	1,0735	-	-	-	-	.....	-	.....	-	.....	-
2	0,97891	1,4383	-	-	-	.....	-	.....	-	.....	-
3	0,93045	1,4142	1,9605	-	-	.....	-	.....	-	.....	-
4	0,67269	1,049	1,5829	2,53	-	.....	-	.....	-	.....	-
5	0,56439	0,95317	1,4601	2,174	3,2377	.....	-	.....	-	.....	-
⋮	⋮	⋮	⋮	⋮	⋮						
10	0,30871	0,42032	0,67167	1,0588	1,6223	.....	7,8727	.....	-	.....	-
⋮	⋮	⋮	⋮	⋮	⋮						
20	0,13366	0,18821	0,26398	0,48466	0,75592	....	3,8128	.....	23,165	.....	-
⋮	⋮	⋮	⋮	⋮	⋮		⋮		⋮		
30	0,0566	0,08182	0,12717	0,32954	0,55871	.....	2,8359	.....	17,3	.....	85,229

7.2.3.1 Effect of varying τ_{app}/μ_1

Figure 7.7 shows the variation of tip shear stress $S_{r\theta}(r = a, \theta = 0)$ as a function of the dimensionless applied or resolved shear stres, τ_{app}/μ_1, for the different in homogeneity types (Γ = 6.88, υ_1 = 0.33 υ_2 = 0.16 Table 7.2) Figure 7.7 shows the discrete nature of dislocation arrays in a pile-up for a constant pile-up length. For constant value of Γ poison ratioes and dimensionless length Λ, the discrete values of dimensionless applied stres, τ_{app}/μ_1, can be calculated by using equation(7.1).

According to Figure 7.7 the size of discontinuty, the change in the tip shear stress when another dislocation is introduced, is lower when dimensionless applied stres increases. As a result, the roll up of a given shear stress at the cylindirical fiber interface need a high resolved shear stres for a SiC fiber. SiC is elastically harder than Al, so the obtained results from Figure 7.7 are satisfied by the general optimization results.

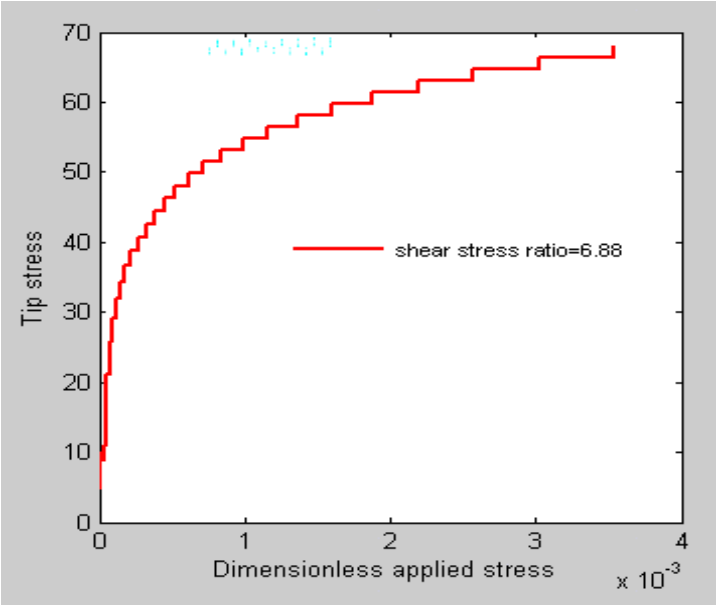

Figure 7.7: Variation of tip stress, S_0, as a function of the applied stres, τ_{app}/μ_1, for the SiC phase (fiber phase) is elastically harder than the matrix ($\Gamma>1$) at constant

7.2.3.2 Effect of changing microstructure, varying Λ

Figure 7.8 shows the variation of tip shear stress $S_{r\theta}(r = a, \theta = 0)$ as a function of the dimensionless pile-up length, Λ, for different stresses and at constant Γ, υ_1, υ_2. The discrete, discontinuous for different applied stress values, τ_{app}/μ_1, shows that the discrete nature of the dislocations in a pile-up.

For a constant shear stres ratio, Γ = 6.88. A critical value of Λ can be defined which there would not be any dislocation. When the defined critical value of Λ exceeded, then one dislocation is introduced into the pile-up, and contribution to the tip shear stress will include the stress field of dislocation. From figure 7.3 when Λ increased more and more, more and more dislocations are allow in and each of contributes to the local stres buildup in a discontinuity way will be a result of a discontinuity at values of Λ pertaining to a different number of dislocations [5]. For constant values Γ = 5.85, υ_1 = 0.33 υ_2 = 0.22 and constant dimensionless applied stress τ_{app}/μ_1, the discrete values of dimensionless pile-up length, Λ, were calculated by using equation (7.2).

The maximum value of the dimensionless pile-up length for an array of *i* dislocations is supposed to be equal to that of the minimum value for *i* + 1 dislocations. We can say that when τ_{app}/μ_1 increased the critical dimensionless plie-up length is decreasing

in Figure 7.8. Increasing τ_{app}/μ_1, does not affect the dimensionless standoff values, since the solution is a function only of the composite variables, but increases N that can be seen as an increasing number of steps in the discrete representation. Thus, the S vs Λ curves shift to higher values for increasing τ_{app}/μ_1.

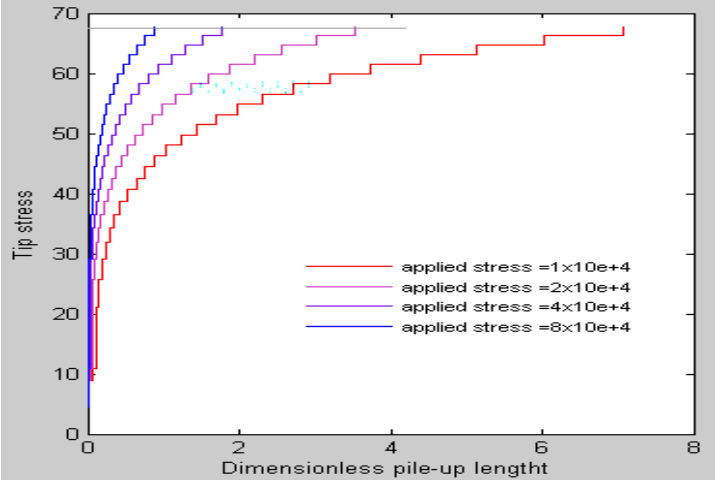

Figure 7.8: Variation of the tip stres, S_0, as a function of dimensionless pile-up length, Λ, for $\Gamma = 6.88$, $\upsilon_1 = 0.33$ $\upsilon_2 = 0.16$.

REFERENCES

[1] **Bulatov V, V. and Cai W.,** 2006. Computer simulations of dislocations, Oxford University Press, London.

[2] **Xiang, Y.,** 2006. Modeling Dislocations at Different Scales, *Communications in computational physics,* **3,** 383-424

[3] **J. Frenkel, Z.,** Physics., 1926. **37** pp. 572 Germany.

[4] The Dislocations Gallery, 3D Simulation of Dislocation Dynamics at the Mesoscopic Scale, <http://zig.onera.fr/DisGallery/>, accessed at 02.12.2008.

[5] **Öveçoğlu, M. L., Barnett, D. M. and Nix, W. D.,** 1986. Analysis of the interfacial stresses produced by a pile-up of discrete edge dislocations in two phase materials, *Acta metall.* **7**, 1779-1789.

[6] **Eshelby, J. D., Frank, F. C. and Nabarro, F. R. N.,** 1951. Phil. Mag. 42, 351, Paris.

[7] **Stroh, A. N.,** 1954. Advances in Physics, Proc. R. Sot. A223, 404.

[8] **Leibfried, G.,** Z. 1951. Physics. pp. 130, 214, Germany.

[9] **Ioakimidis, N. I.,** 1980. On the Natural Interpolation Formula for Cauchy Type Singular Integral Equations of the First Kind, *Computing,* **26,** 73-77

[10] Metal Matrix Composite, <http://en.wikipedia.org/wiki/Metal_matrix_composite>, accesed at 03.12.2008.

[11] **Jones, M. R.,** 1998. Mechanics of Composite Materials Second Edition, Blacksburg, Virginia.

[12] Australian Academy of Science, What makes a material a composite?, <http://www.science.org.au/nova/059/059key.htm>, accessed at 03.12.2008.

[13] **Ünal, N.,** 2006. The effect of boron carbide addition on the structural and mechanical properties of tungsten matrix composites, M.sc. Thesis, ITU Institute of Science, Istanbul.

[14] Dokuwiki Materials Engineering, Clasification of Composites, <http://www.substech.com/dokuwiki/doku.php?id=classification_of_composites>, accessed at 07.12.2008.

[15] **Clyne, T. W. and Withers, P. J.,** 1992. An Introduction to Metal Matrix Composites, Cambridge Solid State Science Series, Cambridge.

[16] Composites-by-Design, Metal Matrix Composites, < http://www.composites-by-design.com/metal-matrix.htm>, accessed at 05.12.2008.

[17] Composite Metal Technologies, Metal Matrix Composites, < http://www.cmt-ltd.com/html/mat_1.htm>, accessed at 12.12.2008.

[18] Energy Programme, Ceramic Matrix Composites, <http://www.ms.ornl.gov/programs/energyeff/cfcc/iof/chap24-6.pdf>, accessed at 12.12.2008.

[19] **Lemaitre, J.,** 2001. Handbook of materials behavior models, Academic Press, New York.

[20] **Naslain, R.,** 1992. Ceramic Matrix composites, Université Bordeaux Press, Glasgow.

[21] Sri Consulting Business Intelligence, Polymer-Matrix Composites, < http://www.sric-bi.com/Explorer/PMC.shtml>, accesed at 13.12.2008.

[22] Composite Materials, Particle-reinforced Composites, <http://science.jrank.org/pages/1665/Composite-Materials-Particle-reinforced-composites.html >, accessed at 17.01.2009.

[23] Official Magazine of the American Composites Manufacturers Association, Composites Manufacturing, <http://www.autocomposites.org/resources/CM_Aug_2007.pdf >, accessed at 14.01.2009.

[24] **Saito, T.,** 1995. A Cost-Effective P/M Titanium Matrix Composite for Automobile Use, *Advanced Performance Materials,* **2**, 121-144

[25] NASA, National Aeronautics and Space Administration, Uncertainties in the Thermal and Mechanical Properties of Particulate Composites Quantified, <http://www.grc.nasa.gov/www/rt/rt2000/5000/5920murthy2.html>, accessed at 16.12.2008.

[26] **Datoo, H. M.,** 2000. Mechanics of Fibrous Composites, Department of Civil and Structural engineering, South Bank Polytechnic, London.

[27] **Ian J. D.,** 1987. Applications of composite materials, Department of Mechanical Engineering, Curtin University of Technology, GPO Box, Perth, WA 6845, Australia.

[28] **Jastrzebski, Z. D. and Wiley, J.,** 1987. The Nature and Properties of Engineering Materials, John Wiley & Sons, 3rd Ed., New York.

[29] **Demirkol, M.,** 2006. Malzemelerin Mekanik Davranışı, Lecturer Notes, Istanbul.

[30] **Dieter, G. E.,** 1988. Mechanical Metallurgy, SI Metric Ed., McGraw Hill, London,

[31] **Reed-Hill, Robert, E.,** 1973. Physical Metallurgy Principles, Reed-Hill, New York.

[32] Wikipedia, Dislocations**,** <http://en.wikipedia.org/wiki/Dislocation>, accessed at 14.12.2008.

[33] **Hull D. and Bacon J. D,** 2001. Introduction to Dislocations, Forth Edition, Cambridge press, Liverpool.

[34] Structural Imperfections (defects) in Crystalline solids, <www.ce.metu.edu.tr/~ce241/8.%20Structural %20Imperfections.ppt>, accessed at 12.12.2008.

[35] **Read, W. T.,** 1953. Dislocations in Crystals, McGraw-Hill Book Company, New York.

[36] Materials Database, Strusture <http://www.eng.ku.ac.th/~mat/MatDB/MatDB/SOURCE/Struc/xtal/xtal.htm>, accessed at 14.12.2008.

[37] **Hertzberg, R. W.,** 1976. Deformation and Fracture Mechanics of Engineering Materials, Wiley, New York.

[38] **Sadd, M. H.,** 2005. Elasticity theory, applications and numerics, Department of Mechanical Engineering and Applied Mechanics Kingston, Rhode Island, Amsterdam.

[39] **Janssens K. G. F., Raabe D. and Kozeschnik E.,** 2006. Computational Materials Engineering an Introduction to Microstructure Evolution, Elsevier Inc, Switzerland.

[40] **Ugural, A.C. and Fenster, S.K.,** 2003. Advanced Strength and Applied Elasticity, 4th editon, Prentice Hall PTR, London.

[41] **Symon, K.,** 1971. Mechanics, Addison-Wesley, New York.

[42] **Hirth, J. P. and Lothe J.,** 1982. Theory of Dislocations Second edition, New York.

[43] Mathworks, Symbolic Math Toolbox 5.1**,** <http://www.mathworks.com/products/symbolic/>, accessed at 15.12.2008.

[44] **Öveçoğlu, M. L.,** 1993. Fiber Kompozitlerde Dislokasyon Yığılması, 7th. International Material and Metallurgy Conference, Ankara.

[45] Mathworks, Optimization Toolbox 4.1, <http://www.mathworks.com/products/optimization/>, accessed at 16.12.2008.

[46] **Rao, S. S.,** 1996. Engineering optimization Theory and practice, School of Mechanical Engineering, Purdue University West Lafayette, Indiana,

[47] **Bazaraa, M. S., Sherali H. D. and Shetty C. M.,** 2006. Nonlinear programming, Third edition, John Wiley & Sons, Inc., New York USA,

[48] Mathworks, Constrained Nonlinear Optimization, <http://www.mathworks.com/access/helpdesk/help/toolbox/optim/index.html?/access/helpdesk/help/toolbox/optim/ug/brnoxr71.html>, accessed at 16.12.2008.

[49] Mathworks, Unconstrained Nonlinear Optimization, Optimization Toolbox <http://www.mathworks.com/access/helpdesk/help/toolbox/optim/index.html?/access/helpdesk/help/toolbox/optim/ug/brnoxr71.html&http://www.mathworks.com/access/helpdesk/help/toolbox/optim/ug/fminunc.html#brnpcy5>, accessed at 16.12.2008.

[50] **More, J.J. and Sorensen, D. C.,** 1983. Computing a Trust Region Step, *SIAM Journal on Scientific and Statistical Computing*, **3**, 553-572.

[51] **Coleman, T.F. and A. Verma,** 2005. A Preconditioned Conjugate Gradient Approach to Linear Equality Constrained Minimization, Cornell University Press, USA.

[52] **Sorensen, D.C.,** 1994. "Minimization of a Large Scale Quadratic Function Subject to an Ellipsoidal Constraint," Department of Computational and Applied Mathematics, Rice University, Technical Report TR94-27.

[53] Efunda Engineering Fundamental, Basic Mechanical Properties, <http://www.efunda.com/materials/common_matl/Common_matl.cfm ?MatlPhase= Solid&MatlProp=Mechanical#Mechanical>, accessed at 16.2.2009.

[54] Material Science and Engineering Labrotuary, Sintered Silicon Carbide(SiC), <http://www.ceramics.nist.gov/srd/summary/ scdscs.htm>, accessed at 16.12.2008.

[55] Scientific Background of Diamonds, The Physical Magnitudesn, Gand E, <http://www.worldgemology.org:8080/ClientZone/Trade/book/chapter7/Page2.aspx>, accessed at 16.12.2008.

APPENDIX A

Airy function in cartessian and polar coordinates was calculated by following codes. Symbolic.m file is a code to obtain symbolic variables for $\sigma_{rr}, \sigma_{\theta\theta}, \sigma_{r\theta}$. Symbolic_hessian.m file is a code to obtain hessian matrix for object function. Object function obtained numerically in appendix B.

```
 **symbolic.m %symbolic codes written to calculate symbolic values of σ_rr, σ_θθ, σ_rθ
clc
clear
%%created by hayri sezer
%% airy_fun function in cartesian coordinates.
%mu1 mu2 shear stress for two different phase.
% k1= 3-v1 v1, v2 are poison ratio for two different phase
% x y are cartesian coordinates.
%l lambda a:radius of the fiber
% defination of variables for symbolic math tool
syms x y l a C1 C2 C3 mu1 b k1 theta
%fi1 is a subfunction of airy_fun function in cartesian coordinates.
fi1=0.5*log((x-l*a)^2+y^2)*y;
%show fi1 in symbolic math tool box
%pretty(fi1);
%fi2 is a subfunction of airy_fun function in cartesian coordinates.
fi2=0.5*C1*y*log(((x-a/l)^2+y^2)/(x^2+y^2));
%show fi2 in symbolic math tool box
%pretty(fi2);
%fi3 is a subfunction of airy_fun function in cartesian coordinates.
fi3=C2*((x-a/l)*(atan(y/(x-a/l))-atan(y/x)));
%show fi3 in symbolic math tool box
%pretty(fi3);
%fi4 is a subfunction of airy_fun function in cartesian coordinates.
fi4=C3*(((((l^2-1)*a)/(l^3)))*((y*(x-a/l))/(((x-a/l)^2+y^2)^1.5)-...
((l^2-1)*a/l)*(y/((x-a/l)^2+y^2)))+(a^2*y/(x^2+y^2)));
%show fi4 in symbolic math tool box
%pretty(fi4);
%airy_fun function as a function of fi1, fi2, fi3, fi4
constant=-2*mu1*b/(pi*(k1+1));
airy_fun=constant*(fi1+fi2+fi3-fi4);
%show airy_fun function in symbolic math tool box
pretty(airy_fun);
%% jacobian in cartesian coordinates for airy_fun function
J=jacobian([airy_fun],[x y]);
sigmaxy=-jacobian([J(1,2)],[x]);
sigmarrthethe=subs(sigmaxy,[x,y],[a*cos(theta),a*sin(theta)])
sigmaxy_0=subs(sigmaxy,y,0); %(x>=a, y=0) in glide plane condition.
pretty(sigmaxy_0);
%% airy_funpolar is airy_fun function in polar coordinates.
%defination of symbolic variables. r and theta : are axes in polar
```

```
%coordinates.
syms theta r
x=r*cos(theta); % x in polar coordinates
y=r*sin(theta); % y in polar coordinates
% fip1, fip2, fip3, fip4 are subfunction of airy_funpolar function
fip1=0.5*log((x-l*a)^2+y^2)*y;
pretty(fip1);
fip2=0.5*C1*y*log(((x-a/l)^2+y^2)/(x^2+y^2));
pretty(fip2);
fip3=C2*((x-a/l)*(atan(y/(x-a/l))-atan(y/x)));
pretty(fip3);
fip4=C3*(((((l^2-1)*a)/(l^3)))*((y*(x-a/l))/(((x-a/l)^2+y^2)^1.5)-...
((l^2-1)*a/l)*(y/((x-a/l)^2+y^2)))+(a^2*y/(x^2+y^2)));
pretty(fip4);
%airy_funpolar is a function of fip1, fip2, fip3 and fip4.
airy_funpolar=((constant)*(fip1+fip2+fip3-fip4));
pretty(airy_funpolar);
%% partial derrivative of airy_funpolar function respect to r and theta
%jacobian(f,v) computes the Jacobian of the scalar or vector f with respect
%to v. The (i,j)-th entry of the result is . Note that when f is scalar,
%the Jacobian of f is the gradient of f. Also, note that v can be a scalar,
%although in that case the result is the same as diff(f,v).
Jrtheta=jacobian([airy_funpolar],[r theta]);
pretty(Jrtheta);
% Jrtheta is a matrix (1x2) Jrtheta(1,1) is derivative of the airy_funpolar
% respect to r.
% sigmathetathea is the second derivative of airy_funpolar function respect to r
sigmathetatheta=jacobian([Jrtheta(1,1)],[r]);
pretty(sigmathetatheta);
%sigmartheta is derivative of the first derivation of the airy_funpolar respect
%theta to r.
sigmartheta=-jacobian([(1/r)*Jrtheta(1,2)],[r]);
pretty(sigmartheta);
%sigmart_0 is stress of r>=a and theta=0
sigmart_0=subs(sigmartheta,theta,0);
pretty(sigmart_0);
sigmarr=(1/r)*Jrtheta(1,1)+(1/r^2)*jacobian([Jrtheta(1,2)],[theta]);
pretty(sigmarr);
sigmaxyp_0=2*mu1*b/pi/(k1+1)*(1/2*(2*x-2*l*a)/(x-l*a)^2+1/2*C1*...
    ((2*x-2*a/l)/x^2-2*(x-a/l)^2/x^3)/(x-a/l)^2*x^2+C2*...
    (1/(x-a/l)-1/x)+C2*(x-a/l)*(-1/(x-a/l)^2+1/x^2)...
    -C3*((l^2-1)*a/l^3*(1/((x-a/l)^2)^(3/2)-3/2*(x-a/l)...
    /((x-a/l)^2)^(5/2)*(2*x-2*a/l)+(l^2-1)*a/l/...
    (x-a/l)^4*(2*x-2*a/l))-2*a^2/x^3));
sigmarty_0=subs(sigmaxyp_0,theta,0);
fprintf('==========================================================================\n')
fprintf('sigmartheta= \n')
pretty(sigmarty_0);
fprintf('============================tipstress=====================================\n')
fprintf('tipstress= \n')
sigmar_atheta=subs(sigmaxyp_0,[r,theta],[a,0]);
pretty(sigmar_atheta);
```

```
%*symbolic_hessian.m
syms xi xj C1 C2 C3
              A=1/(xj-xi);
              B=-C1*((1/xj)-(xi/(xi*xj-1)));
              C=-C2*((1/(xi*xj^2)));
              D=2*C3*(((xi^2-1)/(xi*(xi*xj-1))^2)-...
              (((xi^2-1)^2)/(xi*(xi*xj-1)^3)))+2*C3/xj^3;
              f=A+B+C+D;
J=jacobian([f],[xi,xj]);
fprintf('=====================================================\n')
pretty(J(1,1))
fprintf('=====================================================\n')
pretty(J(1,2))
FH=hessian(f,[xi xj]);
fprintf('=====================================================\n')
pretty(FH(1,1))
fprintf('=====================================================\n')
pretty(FH(2,2))
fprintf('=====================================================\n')
pretty(FH(2,1))
fprintf('=====================================================\n')
pretty(f)
fprintf('=====================================================\n')
```

APPENDIX B

Numerical part of computational process calculated in the following codes. Firstly airy function was written as a function in matlab tezfgHessian.m as a matlab function. Hessian of airy function was obtained in appendix A. Then the obtained values for hessian matrix used in the matlab function in the tezfgHessian. A general code in generaloptimization.m was written to optimize general objective function which calculated in tezfgHessian.m.

Variation of tipstress as a function of dimensionless pile-up length calculated in pile_up.m file for general optimization result and the other three cases. Pile_up.m file is a general code for all cases. To calculate variation of tipstress as a function of dimensionless pile-up length for Al/SiC, Al/Al_2O_3 and Cu/WC the specific parameters namely, shear stress and poison ratios was got from Table 7.2. Appliedstress.m file is a general code for all cases. To calculate variation of tipstress as a function of dimensionless appliedstress for Al/SiC, Al/Al_2O_3 and Cu/WC the specific parameters namely, shear stress and poison ratios was got from Table 7.2.

```
% this is a matlab function. It is objective function of airy function
function [F,G]  = tezfgHessian(x)
%objective function
nu1=0.33; nu2=0.22; a=1; tapp=1; b=1; kappa =5.85; k1=3-4*nu1; k2=3-4*nu2;
alpha=(kappa*(k1+1)-(k2+1))/(kappa*(k1+1)+(k2+1));
beta=(kappa*(k1-1)-(k2-1))/(kappa*(k1+1)+(k2+1));
C1=(alpha+beta^2)/(1-beta^2); C2=((1+alpha)*beta)/(1-beta^2);
C3=(beta-alpha)/(2*(4+beta)); R=a*pi*(k1+1)*tapp/(2*1*b);
j=length(x); A=zeros(j,1); B=zeros(j,1); C=zeros(j,1); D=zeros(j,1);
        for i=1:j
            if i~=j
                A(i)=1./(x(j)-x(i));
            end
                B(i)=x(i)/(x(i)*x(j)-1);
                C(i)=-C2*((1/(x(i)*x(j)^2)));
                D(i)=(((x(i)^2-1)/(x(i)*(x(i)*x(j)-1))^2)-...
                (((x(i)^2-1)^2)/(x(i)*(x(i)*x(j)-1)^3)));
        end
        f=sum(A)-C1*((1/x(j))-sum(B))+sum(C)+2*C3*((1/x(j)^3)+sum(D))-R;
        F=(f^2);
        if nargout>1
        G=zeros(j,1);
        for i=1:j
```

```
            if i~=j
            G(i)=(1/(x(i)^2-x(j)^2))-C1*(-(1/(x(i)*x(j)))+...
                ((x(i)*x(j))/((x(i)*x(j)-1)^2)))+C2/(x(i)^2*x(j)^2)+...
                2*C3*(2/(x(i)*(x(i)*x(j)-1)^2)-2*(x(i)^2-1)/...
                (x(i)^3*(x(i)*x(j)-1)^2)-((2*(x(i)^2-1)*x(j))/...
                (x(i)^2*(x(i)*x(j)-1)^3))-(4*(x(i)^2-1)/(x(i)*x(j)-1)^3)+...
                ((x(i)^2-1)^2/(x(i)^2*(x(i)*x(j)-1)^3))+...
                (3*(x(i)^2-1)^2*x(j)/(x(i)*(x(i)*x(j)-1)^4)));
            G(j)=(-1/(x(j)-x(i)))^2-C1*((-1/x(j)^2)+(x(i)^2/...
                (x(i)*x(j)-1)^2))+(2*C2/(x(i)*x(j)^3))+...
                2*C3*((-2*(x(i)^2-1)/(x(i)*(x(i)*x(j)-1)^3))+...
                (3*(x(i)^2-1)^2/(x(i)*x(j)-1)^4))-(6*C3/x(j)^4);
            end
        end
end

%**generaloptimization.m***
%created by Hayri Sezer
%call objection function for optimization process.
%xstart is the initial value of system.
clc, clear
n = input('enter number of dislocations  n= ');
h_1=8; h_2=10; h_3=16;
for j=1:n
    x=zeros(n,j); xstart=-zeros(j,1); tt = -zeros(n,j);
    xstart(1,1)=1.23; xxstart(1,1)=1.17;
    for i=1:j
        if i>1 && i<h_1
        xstart(i,1)=xstart(i-1,1)*(1.5+1.5*0.02);
        end
         if i>=h_1 && i<h_2
            xstart(i,1)=xstart(i-1,1)*(1.3+1.3*0.02);
         end
         if i>=h_2 && i<h_3
            xstart(i,1)=xstart(i-1,1)*(1.2+1.2*0.02);
         end
         if i>=h_3
            xstart(i,1)=xstart(i-1,1)*(1.15+1.15*0.02);
         end
    end
    if j<h_1
        tt=xstart*(1/j^0.42);
G=sparse(1:1,1:1,1,j,j); T=-sparse(1:j,1:j,1,j,j); TT=sparse(2:j,1:j-
1,1.2,j,j);
A=G+T+TT; b=ones(j,1)*0.005; lb=ones(j,1).*tt*0.08; fff=sparse(1:j-
1,1,1,j,1)*1.2.*tt;
ggg=sparse(j:j,1,1,j,1)*3.*tt; ub=fff+ggg;

options = optimset('LargeScale','on','TolFun',1e-010,'TolX',1e-06,...
    'MaxFunEvals',10000,'MaxIter',10000);
[yyy,fval] = fmincon(@tezfgHessian,tt,A,b,[],[],lb,ub,[],options);
    end
    if j>=h_1 & j<h_2
        tt=xstart*(1/j^0.51); G=sparse(1:1,1:1,1,j,j); T=-
sparse(1:j,1:j,1,j,j);
TT=sparse(2:j,1:j-1,1.2,j,j); A=G+T+TT; b=ones(j,1)*0.005;
lb=ones(j,1).*tt*0.08;
fff=sparse(1:j-1,1,1,j,1)*1.2.*tt; ggg=sparse(j:j,1,1,j,1)*3.*tt; ub=fff+ggg;
```

```
options = optimset('LargeScale','on','TolFun',1e-010,'TolX',1e-06,...
    'MaxFunEvals',10000,'MaxIter',10000);
[yyy,fval] = fmincon(@tezfgHessian,tt,A,b,[],[],lb,ub,[],options);
    end
    if j>=h_2 && j<h_3
        tt=xstart*(1/j^0.62); G=sparse(1:1,1:1,1,j,j); T=-
sparse(1:j,1:j,1,j,j);
TT=sparse(2:j,1:j-1,1,j,j); A=G+T+TT; b=ones(j,1)*0.005;
lb=ones(j,1).*tt*0.08;
fff=sparse(1:j-1,1,1,j,1)*1.2.*tt; ggg=sparse(j:j,1,1,j,1)*3.*tt; ub=fff+ggg;
options = optimset('LargeScale','on','TolFun',1e-010,'TolX',1e-06,...
    'MaxFunEvals',10000,'MaxIter',10000);
[yyy,fval] = fmincon(@tezfgHessian,tt,A,b,[],[],lb,ub,[],options);
    end
     if j>=h_3
        tt=xstart*(1/j^0.73); G=sparse(1:1,1:1,1,j,j); T=-
sparse(1:j,1:j,1,j,j);
TT=sparse(2:j,1:j-1,1,j,j); A=G+T+TT; b=ones(j,1)*0.005;
lb=ones(j,1).*tt*0.08;
fff=sparse(1:j-1,1,1,j,1)*1.2.*tt; ggg=sparse(j:j,1,1,j,1)*3.*tt;
ub=fff+ggg; options = optimset('LargeScale','on','TolFun',1e-010,'TolX',1e-
06,...
    'MaxFunEvals',10000,'MaxIter',10000);
[yyy,fval] = fmincon(@tezfgHessian,tt,A,b,[],[],lb,ub,[],options);
    end
    ty=sparse(j,1:j,tt,n,n);  tty(j,:)=ty(j,:);
tfval=sparse(j,n+1,fval,n+1,n+1);
    tr=sparse(j,1:j,yyy,n+1,n+1);  ff(j,:)=tr(j,:)+tfval(j,:);
yy(j,:)=tr(j,:);
    trr=sparse(j,1:j,ub,n,n); ttyy(j,:)=trr(j,:);  trrr=sparse(j,1:j,lb,n,n);
    ttyyy(j,:)=trrr(j,:);
end
dd=full(ff); y=full(yy); transpose_y=y; gggggg=sparse(tty); ddd=full(tty);
diagonal = diag(y);


%***pile_up.m****
%variation of tipstress as a function of dimensionless pile-up length
nu1=0.33; nu2=0.22;
for kk=1:1:4
tapp=input('applied stress: ');
a=1; b=1; kappa =5.85; k1=3-4*nu1; k2=3-4*nu2;
alpha=(kappa*(k1+1)-(k2+1))/(kappa*(k1+1)+(k2+1));
beta=(kappa*(k1-1)-(k2-1))/(kappa*(k1+1)+(k2+1));
C1=(alpha+beta^2)/(1-beta^2); C2=((1+alpha)*beta)/(1-beta^2);
C3=(beta-alpha)/(2*(4+beta)); disnum= input('enter dislocation number  : ');
for n=1:30;
    for i =1:n;
    lema=-((1/(a*(1-transpose_y(i,disnum))))+C1*(transpose_y(i,disnum)/(...
    a*(1-transpose_y(i,disnum))))-(C1/a)-(C2/(transpose_y(i,disnum)*a))+...
      C3*2*(transpose_y(i,disnum).^2-1)*a/(transpose_y(i,disnum)*(...
      a*(1-transpose_y(i,disnum))).^2)-C3*2*(transpose_y(i,disnum...
      ).^2-1)*a/(transpose_y(i,disnum)*(a*(1-
transpose_y(i,disnum))).^3)+(C3*2/a));
end
sigma(n)=sum(lema);
   end
```

```
retaa=cumsum(sigma); beta=retaa'; nu1=0.33; k1=3-4*nu1;
dimensionlesslength=4*0.1*transpose_y(1:30,30)/((pi+k1)*tapp);
stairs (dimensionlesslength(1:30,1),beta(1:30,1)); hold on
end

%**appliedstress.m**
%variation of tip stress as a function of applied stress
nu1=0.33; nu2=0.22;
for kk=1:1:3
    kappa=input('kappa='); %kappa is ratio of shear stress for matrix and
fiber
a=1; tapp=1; b=1; k1=3-4*nu1; k2=3-4*nu2;
alpha=(kappa*(k1+1)-(k2+1))/(kappa*(k1+1)+(k2+1));
beta=(kappa*(k1-1)-(k2-1))/(kappa*(k1+1)+(k2+1));
C1=(alpha+beta^2)/(1-beta^2); C2=((1+alpha)*beta)/(1-beta^2);
C3=(beta-alpha)/(2*(4+beta)); disnum= input('enter dislocation number  : ');
for n=1:30;
for i =1:n;
   lema=-((1/(a*(1-transpose_y(i,disnum))))+C1*(transpose_y(i,disnum)/(a*(...
        1-transpose_y(i,disnum))))-(C1/a)-(C2/(transpose_y(i,disnum)*a))+...
        C3*2*(transpose_y(i,disnum).^2-1)*a/(transpose_y(i,disnum)*(a*(...
        1-transpose_y(i,disnum))).^2)-C3*2*(transpose_y(i,disnum).^2-...
        1)*a/(transpose_y(i,disnum)*(a*(1-
transpose_y(i,disnum))).^3)+(C3*2/a));
end
sigma(n)=sum(lema);
end
retaa=cumsum(sigma); beta=retaa'; nu1=0.33; k1=3-4*nu1;
appliedstres=2*transpose_y(1:30,30)/((pi+k1)*10000);
stairs (appliedstres(1:30,1),beta(1:30,1));
hold on
end
```

CURRICULUM VITAE

Candidate's full name: Hayri SEZER

Place and date of birth: Adıyaman/Gölbaşı 01.09.1983

Permanent Address: Şirinevler Mah. Fetih Sk. No: 5/4 Bahçelievler/İstanbul

Universities and
Colleges attended: İstanbul Technical University, Faculty of Science & Letter, Department of Physics Engineering, 2005.